Measurement of the Z boson production cross-section in proton-lead collisions at $\sqrt{s_{\mathrm{NN}}} = 8.16$ TeV

The LHCb collaboration

E-mail: hengne.li@m.scnu.edu.cn

ABSTRACT: This article presents the first measurement of the differential Z-boson production cross-section in the forward region using proton-lead collisions with the LHCb detector. The dataset was collected at a nucleon-nucleon centre-of-mass energy of $\sqrt{s_{\mathrm{NN}}} = 8.16$ TeV in 2016, corresponding to an integrated luminosity of $30.8\,\mathrm{nb}^{-1}$. The forward-backward ratio and the nuclear modification factors are measured together with the differential cross-section as functions of the Z boson rapidity in the centre-of-mass frame, the transverse momentum of the Z boson and a geometric variable ϕ^*. The results are in good agreement with the predictions from nuclear parton distribution functions, providing strong constraining power at small Bjorken-x.

Contents

1   Introduction

Inclusive Z-boson[1] production at hadron colliders [1] is an important benchmark process to test quantum chromodynamics (QCD), and can be factorised [2] as a product of the hard scattering and the initial state of the collision. State-of-the-art next-to-next-to-leading order (NNLO) calculations in perturbative QCD (pQCD), together with next-to-next-to-leading logarithm (NNLL) resummation [3–10] and next-to-leading order (NLO) electroweak (EW) corrections [11–13], precisely describe the hard process, while the non-perturbative initial-state can be be modelled through parton distribution functions (PDF) [14, 15] or nuclear PDFs (nPDF) [16–21]. As a result, Z-boson production at the Large Hadron Collider (LHC) carries valuable information in constraining the PDFs and nPDFs. Weakly coupled Z bosons and their leptonic decay final states have a negligible interaction with the nuclear medium and can be used as clean probes of nuclear-matter effects on the initial-state. The production of Z bosons is sensitive to only the initial-state, while hadronic probes are sensitive to both initial- and final-state nuclear matter effects. Therefore, together with hadronic probes Z-boson production can differentiate between effects of the initial- and final-state. Studies [16] also show that Z-boson production in

---

[1]In this paper, the label Z boson is defined to include contributions from virtual photons.

proton-lead (pPb) collisions at the LHC is sensitive to heavier quark flavours. Improved information on the nuclear corrections is helpful to reduce proton PDF uncertainties and essential for distinguishing the distributions for the different parton flavours. Moreover, Z-boson production is an ideal process to probe transverse-momentum-dependent PDFs (TMDs) [22–25] when its transverse momentum is below $\sim 10\,\text{GeV}$, where non-perturbative QCD effects start to dominate [26].

The LHCb experiment published for the first time the inclusive Z production result in the forward region in pPb collisions at a nucleon-nucleon centre-of-mass energy $\sqrt{s_{\text{NN}}} = 5.02\,\text{TeV}$ [27]. The unique forward geometry coverage allows the LHCb detector to probe nPDFs at very small Bjorken-x ($10^{-4} < x < 10^{-3}$). This measurement was followed by the inclusive and differential results in the central region from the CMS and ATLAS experiments [28, 29] and in the forward region from the ALICE experiment [30] at $\sqrt{s_{\text{NN}}} = 5.02\,\text{TeV}$. Inclusive and differential results are also measured at $\sqrt{s_{\text{NN}}} = 8.16\,\text{TeV}$ by the CMS collaboration in the central region [31] and by the ALICE collaboration in the forward region [32]. These results are in good agreement with NLO pQCD predictions calculated with commonly used nPDFs such as EPPS09 [17] and nCTEQ15 [33].

This article presents the first differential measurement of the production cross-section, the forward-backward ratio of the production cross-sections and the nuclear modification factors of $Z \to \mu^+\mu^-$ production with the LHCb experiment using pPb collisions. The dataset was collected at $\sqrt{s_{\text{NN}}} = 8.16\,\text{TeV}$ in 2016. The inclusive cross-sections in the proton-lead (forward) and lead-proton (backward) collisions are measured, together with the differential cross-sections as a function of the rapidity of the Z boson in the centre-of-mass frame (y_Z^*), the transverse momentum (p_{T}^Z) and an angular variable ϕ^* [34]. The ratio between the cross-sections in forward and backward collisions in a common rapidity range (R_{FB}) and the nuclear modification factors ($R_{p\text{Pb}}$) with respect to pp collisions are measured, both inclusively and differentially as functions of the above three variables.

2 Detector, datasets, and theoretical predictions

The LHCb detector [35, 36] is a single-arm forward spectrometer covering the pseudorapidity (η) range from 2 to 5. The detector includes a high-precision tracking system consisting of a silicon-strip vertex detector surrounding the pp interaction region, a large-area silicon-strip detector located upstream of a dipole magnet with a bending power of about $4\,\text{Tm}$, and three stations of silicon-strip detectors and straw drift tubes placed downstream of the magnet. The tracking system provides a measurement of the momentum, p, of charged particles with a relative uncertainty that varies from 0.5% at low momentum to 1.0% at $200\,\text{GeV}$. Natural units with $\hbar = c = 1$ are used throughout. The impact parameter (IP), defined as the minimum distance of a track to a primary vertex (PV), is measured with a resolution of $(15 + 29/p_{\text{T}})\,\mu\text{m}$, where p_{T} is the component of the momentum transverse to the beam, in GeV. Muons are identified by a system composed of alternating layers of iron and multiwire proportional chambers.

This analysis uses pPb collision data at a centre-of-mass energy per nucleon pair of $\sqrt{s_{\text{NN}}} = 8.16\,\text{TeV}$ recorded in 2016 by the LHCb detector, with an energy of $6.5\,\text{TeV}$ for the p

beam and 2.56 TeV per nucleon for the Pb beam. Since the collision system is asymmetric, a detector acceptance of $2.0 < \eta < 4.5$ in the laboratory frame is translated into a muon rapidity (y_μ^*) acceptance of $1.53 < y_\mu^* < 4.03$ in the centre-of-mass frame [2], when the p beam travels towards the positive η direction of the LHCb detector (forward collision). Similarly, when the p beam travels in the negative η direction (backward collision), the muon rapidity acceptance in the centre-of-mass frame is $-4.97 < y_\mu^* < -2.47$. The integrated luminosity is determined [37] to be $12.2 \pm 0.3 \, \mathrm{nb}^{-1}$ for forward collisions and $18.6 \pm 0.5 \, \mathrm{nb}^{-1}$ for backward collisions. For the background and efficiency estimation, pp collisions recorded in 2016 at $\sqrt{s} = 13$ TeV are used, corresponding to an integrated luminosity of $1.7 \, \mathrm{fb}^{-1}$.

Full detector simulation is required to model the detector acceptance effects and selection efficiencies. The pPb collisions are simulated by embedding multiple minimum-bias events generated separately into a $Z \to \mu^+\mu^-$ signal event, so that the multiplicity profile in the simulated events agrees with that of the collision data. The signal $Z \to \mu^+\mu^-$ events are generated with PYTHIA 8 [38, 39] using a specific LHCb configuration and the CTEQ6L1 [40] PDF set with a specific LHCb configuration [41] assuming pp interactions with beam momenta equal to the momenta per nucleon of the p and Pb beams. Decays of unstable particles are described by EVTGEN [42], in which final-state radiation is generated using PHOTOS [43]. Minimum-bias events are generated using the EPOS event generator with the LHC model [44]. The interaction and the response of the generated particles with the detector are implemented using the GEANT4 toolkit [45, 46], as described in ref. [47].

The results of the analysis are compared to theory predictions determined at fixed order in pQCD and given by the POWHEGBOX v2 [48–51] generator, which calculates the hard interaction using pQCD at NLO. The POWHEGBOX package is interfaced with the LHAPDF package [52] to supply different (n)PDF sets for describing the non-perturbative initial states. PDF sets CT14 [53] and CTEQ6.1 [54] are used for the p side of the pPb collisions, and nPDF sets EPPS16 [17, 53] and nCTEQ15 [33] are used for the Pb side. Choosing CT14 and CTEQ6.1 PDF sets for the p side is motivated by the fact that they are the free proton PDFs used inside the EPPS16 and nCTEQ15 nPDF sets, respectively. The muon rapidity acceptances in pp, in forward and in backward pPb collisions are different, which need to be corrected for the R_{FB} and $R_{p\mathrm{Pb}}$ measurements. The POWHEGBOX generator with the CTEQ6.1 proton PDF is used to derive the corresponding correction factors.

3 Event selection

The online event selection is performed by a trigger, which consists of a hardware stage followed by a two-level software stage. The hardware trigger used in this analysis selects events containing at least one muon with p_{T} greater than 500 MeV. In the first stage of the software trigger, at least one muon with p_{T} greater than 1.3 GeV and p greater than 6.0 GeV is required. Alignment and calibration of the detector are performed in near real-time [55]. The same alignment and calibration information is propagated to the offline

---

[2]When the momentum of a particle is much greater than its mass, its rapidity is approximately equal to its pseudorapidity $(y \sim \eta)$.
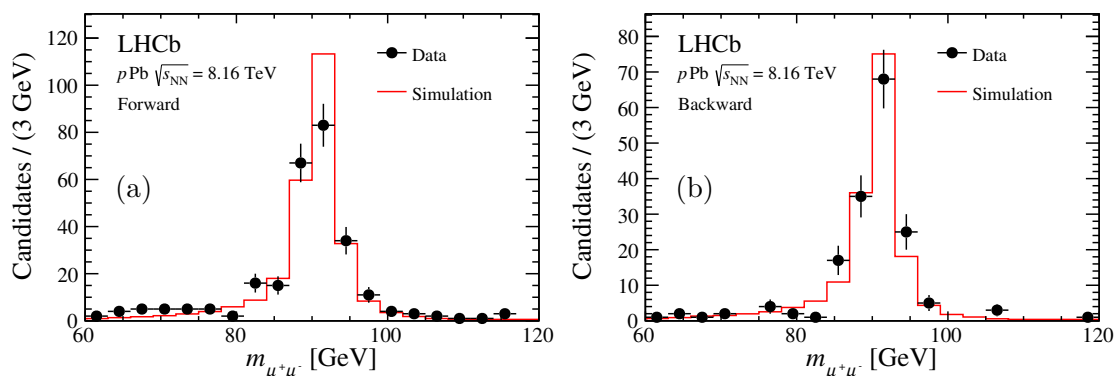
Figure 1. Dimuon invariant mass of the selected events for (a) forward and (b) backward collisions, respectively. The red histograms show the distributions from simulation normalised to the number of observed candidates.

reconstruction, ensuring consistent and high-quality particle identification information between the trigger and the offline software. The present analysis is performed directly using candidates reconstructed at the trigger stage [56, 57], owing to the identical performance of the online and offline reconstruction.

The second software-trigger stage and the offline reconstruction level selection require each event to have a PV reconstructed using at least four tracks measured in the vertex detector. For events with multiple PVs, the PV that has the smallest χ^2_{IP} with respect to the selected dimuon candidate is chosen, where χ^2_{IP} is defined as the difference between the vertex-fit χ^2/ndf calculated with and without the two tracks from the dimuon candidate included in the vertex fit. Each identified muon candidate is required to have $p_{\mathrm{T}} > 20\,\mathrm{GeV}$, $2 < \eta < 4.5$ and a good track fit. The two muon tracks of the Z boson candidate must form a good-quality vertex (vertex-fit $\chi^2/\mathrm{ndf} < 25$), representing a tighter selection compared to the software trigger requirement. The dimuon invariant mass is required to be in the range between 60 and 120 GeV. The selected numbers of candidates are 268 and 166 for forward and backward collisions, respectively. The dimuon invariant mass of the selected candidates is shown in figure 1 for both forward and backward collisions. The red histogram shows the distributions of simulated $Z \to \mu^+\mu^-$ events generated using PYTHIA 8 with the CTEQ6L1 [40] PDF set, normalized to the number of observed candidates.

4 Data analysis

This analysis measures the cross-section of the $Z \to \mu^+\mu^-$ production in a fiducial region with $60 < m_{\mu^+\mu^-} < 120\,\mathrm{GeV}$ where both muons satisfy $p_{\mathrm{T}} > 20$ GeV and $2 < \eta < 4.5$. The differential cross-section in the fiducial region is defined as

$$\frac{\mathrm{d}\sigma^{\mathrm{fid}}_{Z \to \mu^+\mu^-}}{\mathrm{d}x} = \frac{\rho(x) \cdot f_{\mathrm{FSR}}}{\mathcal{L} \cdot \epsilon^{\mathrm{reco\&sel}}(x) \cdot \epsilon^{\mathrm{muon\text{-}id}}(x) \cdot \epsilon^{\mathrm{trig}}(x)} \cdot \frac{\mathrm{d}N_{\mathrm{cand}}}{\mathrm{d}x}, \tag{4.1}$$

where N_{cand} is the number of observed candidates after the selection in the fiducial region; ρ is the purity (the fraction of signal events); f_{FSR} is the correction for final state radiation

(FSR); $\mathcal{L}$ is the integrated luminosity; $\epsilon^{\text{reco\&sel}}$, $\epsilon^{\text{muon-id}}$ and ϵ^{trig} are the efficiencies of reconstruction and selection, muon identification and trigger selection, respectively; and x can be y_Z^*, p_T^Z or ϕ^* (applied throughout this section unless stated otherwise). The variable ϕ^* is defined as

$$\phi^* = \frac{\tan(\phi_{\text{acop}}/2)}{\cosh(\Delta\eta/2)}, \tag{4.2}$$

where $\Delta\eta$ is the difference between the pseudorapidity of the two muons, $\phi_{\text{acop}} = \pi - |\Delta\phi|$ is the acoplanarity, with $\Delta\phi$ being the difference between the azimuthal angles of the two muons. The angle ϕ^* was introduced and studied in refs. [34, 58] as an observable complementary to the variable p_T^Z to study the shape of the Z boson transverse-momentum distribution with reduced sensitivity to experimental resolution effects.

The ratio of the $Z \to \mu^+\mu^-$ production cross-sections between forward and backward directions, R_{FB}, is particularly sensitive to nuclear effects. In the case of pp collisions, the R_{FB} is expected to be unity, because the Z boson production cross-section should be symmetric between forward and backward rapidity. However, in the case of pPb collisions, the nuclear modifications are different for forward (small Bjorken-x, $i.e.$, $x < 10^{-3}$) and backward (large Bjorken-x, $i.e.$, $x > 10^{-1}$) rapidity. As such, there is suppression at small Bjorken-x due to nuclear shadowing effects [59], and enhancement at large Bjorken-x because of the EMC effect [60]. Therefore, the R_{FB} is an effective observable to probe nuclear-matter effects.

The forward-backward ratio is determined in the common rapidity range $2.5 < |y_Z^*| < 4.0$ as

$$R_{\text{FB}}(x) = \frac{\mathrm{d}\sigma_{\text{fw}}/\mathrm{d}x}{\mathrm{d}\sigma_{\text{bw}}/\mathrm{d}x} \cdot k_{\text{FB}}(x)\bigg|_{2.5 < |y_Z^*| < 4.0}, \tag{4.3}$$

where σ_{fw} is the cross-section in the forward collisions, and σ_{bw} in the backward collisions. The factor $k_{\text{FB}}(x)$, which corrects for the difference of the muon rapidity acceptance between forward and backward collisions, is determined as

$$k_{\text{FB}}(x) = \frac{\mathrm{d}\sigma'_{(pp,-4.97<y_\mu^*<-2.47)}/\mathrm{d}x}{\mathrm{d}\sigma'_{(pp,1.53<y_\mu^*<4.03)}/\mathrm{d}x}\bigg|_{2.5 < |y_Z^*| < 4.0}, \tag{4.4}$$

using POWHEGBOX with the proton PDF CTEQ6.1. Choosing the proton PDF instead of the nPDF avoids the acceptance correction factor being biased by nuclear modification information encoded in the nPDF. The prime symbol ("σ'") in the equation indicates that this cross-section is calculated theoretically instead of from data measurements.

The nuclear modification factor ($R_{p\text{Pb}}$) for forward and backward collisions is measured as

$$R_{p\text{Pb}}^{\text{fw}}(x) = k_{p\text{Pb}}^{\text{fw}}(x) \cdot \frac{\mathrm{d}\sigma_{(p\text{Pb},1.53<y_\mu^*<4.03)}/\mathrm{d}x}{208 \cdot \mathrm{d}\sigma_{(pp,2.0<y_\mu^*<4.5)}/\mathrm{d}x} \tag{4.5}$$

and

$$R_{p\text{Pb}}^{\text{bw}}(x) = k_{p\text{Pb}}^{\text{bw}}(x) \cdot \frac{\mathrm{d}\sigma_{(p\text{Pb},-4.97<y_\mu^*<-2.47)}/\mathrm{d}x}{208 \cdot \mathrm{d}\sigma_{(pp,-4.5<y_\mu^*<-2.0)}/\mathrm{d}x}, \tag{4.6}$$

respectively, where 208 is the number of binary nucleon-nucleon collisions in pPb collisions. The $k_{p\text{Pb}}$ factor is to correct for the different y_μ^* acceptance between pPb and pp collisions and can be similarly calculated using POWHEGBOX with the proton PDF set CTEQ6.1,

$$k_{p\text{Pb}}^{\text{fw}}(x) = \frac{\mathrm{d}\sigma'_{(pp,2.0<y_\mu^*<4.5)}/\mathrm{d}x}{\mathrm{d}\sigma'_{(pp,1.53<y_\mu^*<4.03)}/\mathrm{d}x} \tag{4.7}$$

and

$$k_{p\text{Pb}}^{\text{bw}}(x) = \frac{\mathrm{d}\sigma'_{(pp,-4.5<y_\mu^*<-2.0)}/\mathrm{d}x}{\mathrm{d}\sigma'_{(pp,-4.97<y_\mu^*<-2.47)}/\mathrm{d}x} \tag{4.8}$$

for forward and backward collisions, respectively. By construction, the nuclear modification factor is expected to be unity if no nuclear matter effects are present, and can be used to extract nuclear modifications when a proton or neutron is confined in the Pb nucleus.

The dominant background contribution in this analysis is from QCD processes. This background has contributions from heavy flavour hadrons decaying to muons and charged hadrons mis-identified as muons. Contributions from other sources, such as $t\bar{t}$, W^+W^- and $Z \to \tau^+\tau^-$ processes, are found to be negligible [61], and are not considered in the present work. Two methods are employed to estimate the QCD background, using pp collision samples weighted to forward or backward pPb collisions according to the multiplicity profiles.

The first method is a "same-sign" technique, based on the property that the yields of positively and negatively charged hadrons are equal in size in the final states. Therefore, the amounts of same-sign and opposite-sign muon-pair candidates that originated from charged hadrons (either mis-identified as muons, or decayed into muons) are the same. By selecting same-sign muon-pair candidates, the amount of QCD background contaminating the selected signal can be determined.

The second method is the ABCD-likelihood technique, see, *e.g.*, refs. [62–64], which is widely used for QCD background estimation in beyond-Standard-Model searches. In this approach two discriminating variables, the vertex-fit χ^2/ndf and muon isolation variable $I_{\text{T}}^{\text{charged}}$, are considered. The vertex-fit χ^2/ndf is used to verify if the pair of muon candidates originates from the same Z decay, otherwise it is classified as QCD background. The muon isolation variable is defined as the fraction of p_{T} carried by the muon candidate over the sum of p_{T} carried by all the tracks in a cone in the $\eta - \phi$ plane with a size of $\Delta R = \sqrt{\Delta\eta^2 + \Delta\phi^2} < 0.5$ around the muon candidate. This variable is used to assess if a muon candidate is surrounded by charged tracks, which characterises a mis-identified hadron or a muon from a charged-hadron decay. A requirement of $I_{\text{T}}^{\text{charged}} > 0.7$ can effectively separate the signal from the QCD background [27]. These two variables are used to separate the dimuon sample into four regions:

(A) vertex-fit $\chi^2/\text{ndf} < 25$ and at least one muon with $I_{\text{T}}^{\text{charged}} > 0.7$,

(B) vertex-fit $\chi^2/\text{ndf} > 70$ and at least one muon with $I_{\text{T}}^{\text{charged}} > 0.7$,

(C) vertex-fit $\chi^2/\text{ndf} < 25$ and both muons with $I_{\text{T}}^{\text{charged}} < 0.7$, and

(D) vertex-fit $\chi^2/\text{ndf} > 70$ and both muons with $I_{\text{T}}^{\text{charged}} < 0.7$,

Quantity	Forward	Backward
N_{cand} (for σ^{fid})	268 ± 16	166 ± 13
N_{cand} (for R_{FB})	160 ± 13	166 ± 13
N_{cand} (for $R_{p\mathrm{Pb}}$)	241 ± 16	166 ± 13
$\rho\,[\%]$	99.69 ± 0.07	99.75 ± 0.08
$\epsilon^{\mathrm{reco\&sel}}\ [\%]$	$87.2\ \pm 2.9$	$72.0\ \pm 2.5$
$\epsilon^{\mathrm{muon\text{-}id}}\ [\%]$	$97.3\ \pm 0.3$	$97.3\ \pm 0.3$
$\epsilon^{\mathrm{trig}}\ [\%]$	$98.3\ \pm 0.6$	$97.1\ \pm 0.6$
$\mathcal{L}\ [\mathrm{nb}^{-1}]$	$12.2\ \pm 0.3$	$18.6\ \pm 0.5$
f_{FSR}	1.025 ± 0.001	1.025 ± 0.001
k_{FB} (for R_{FB})	$0.65\ \pm 0.02$	–
$k_{p\mathrm{Pb}}$ (for $R_{p\mathrm{Pb}}$)	0.706 ± 0.002	1.518 ± 0.003

Table 1. Observed number of candidates, input values and uncertainties for the overall cross-section and the theory corrections with uncertainties for the R_{FB} and $R_{p\mathrm{Pb}}$ measurements.

where $(\mathrm{A + C})$ is the signal selection fiducial volume. The background contamination in the region $(\mathrm{A + C})$ is therefore estimated as $N_{\mathrm{bkg}}(\mathrm{A + C}) = N(\mathrm{C})/N(\mathrm{D}) \cdot N(\mathrm{B + D})$.

While the ABCD method is more sensitive to QCD backgrounds from heavy-flavour decays, and the same-sign method to hadron mis-identification, there is a sizable overlap between the two methods. Consequently, the final QCD background is taken as the sum of the results from the two methods with a subtraction of this duplication. An estimation of the duplication of the two methods is performed by using the same-sign sample as input to the ABCD method. The resulting average purity is $(99.70 \pm 0.07)\%$ and $(99.75 \pm 0.08)\%$ for the forward and backward collisions, respectively. For the differential measurements as functions of y_Z^*, p_{T}^Z, and ϕ^*, the background is estimated in the same way and found to be independent of these variables. The average purities given above for forward and backward collisions are used correspondingly for the differential measurements.

The efficiency cannot be directly derived from the $p\mathrm{Pb}$ dataset because of its small statistical size. The high statistical pp collision dataset is instead chosen as the starting point for efficiency studies. The efficiencies are evaluated in the fiducial region in two steps. In the first step, a tag-and-probe method [65] is used to derive the efficiencies as a function of multiplicity, p_{T}^μ, η^μ, p_{T}^Z and Z boson rapidity in the lab frame (y_Z) from both pp collision data and $Z \to \mu^+\mu^-$ simulation. The ratios between data and simulation are taken as correction functions. In the second step, the $p\mathrm{Pb}$ simulation is weighted to the $p\mathrm{Pb}$ collider data according to the corresponding multiplicity profiles. The correction functions derived in the first step are then used to further weight the $p\mathrm{Pb}$ simulation to correct for the differences between data and simulation. After a series of reweightings, the $p\mathrm{Pb}$ simulation can correctly reproduce the efficiencies of the $p\mathrm{Pb}$ data. The final efficiency to be used for cross-section measurements can be then derived as the fraction of the weighted yields passing the corresponding selection criteria using the weighted $p\mathrm{Pb}$ simulation.

The resulting average efficiencies ($\epsilon^{\mathrm{reco\&sel}}$, $\epsilon^{\mathrm{muon\text{-}id}}$, and ϵ^{trig}) are shown in table 1 for the forward and backward collisions. The much smaller $\epsilon^{\mathrm{reco\&sel}}$ efficiency in the backward

collisions is mainly due to the far larger contamination from charged tracks when the debris of the Pb nucleus travels towards the LHCb detector. The $\epsilon^{\mathrm{reco\&sel}}$ efficiency for the differential measurements varies from 66.6% to 91.2%, depending on the y_Z^*, p_T^Z or ϕ^* variables. The efficiencies $\epsilon^{\mathrm{muon\text{-}id}}$ and ϵ^{trig} show negligible dependencies on these variables and are considered as constants.

The detector resolution can lead to migration of events from one interval to another in the distribution of an observable. The migration effect is studied by examining the ratio of the distributions of the y_Z^*, p_T^Z and ϕ^* observables between generated and reconstructed events using simulation. It is found to be negligible for the observables y_Z^* and ϕ^*, thanks to the excellent angular resolution of the LHCb detector. However, for the variable p_T^Z the migration effect can be as large as $\sim 10\%$. An unfolding correction is applied for the p_T^Z distributions using the RooUnfold [66] software package with an iterative Bayesian approach [67].

Final-state radiation effects can shift certain events out of the kinematic acceptance boundaries. For a fair comparison of the results with theoretical predictions, the FSR correction (f_{FSR}) is applied to the measured result, which is defined as the ratio of the cross-sections with and without the FSR effect turned on calculated using POWHEGBOX together with PYTHIA 8 [38]. The average value of the FSR correction is about 2.5%.

For the nuclear modification factor measurement, the *pp* reference cross-section at 8.16 TeV is interpolated using a third-order polynomial function from the *pp* measurements at 7, 8, and 13 TeV [61, 68–70] by the LHCb experiment. The resulting interpolated total cross-section at 8.16 TeV is (98.1 ± 0.6) pb in the rapidity range $2.0 < y_Z^* < 4.5$, and varies little with respect to the measured central value of 95 pb at 8 TeV [68]. The differential cross-section in intervals of y_Z, p_T^Z and ϕ^* variables is also interpolated in the same way for each interval. The method has been cross-checked via a linear extrapolation using the 7 and 8 TeV points leading to a negligible difference ($< 0.1\%$) in the result.

5 Systematic uncertainties

Sources of systematic uncertainties considered are the background estimation, efficiency modelling, FSR correction, detector resolution correction, integrated luminosity, and theoretical corrections.

The uncertainty from the background estimation is less than 0.1%, and includes the statistical uncertainty of the *pp* collision dataset used in the estimation and the multiplicity weighting. The multiplicity weighting uncertainty is estimated by varying the weighting function within an envelope defined by the statistical fluctuations of the multiplicity profiles of the *pp* and *p*Pb datasets. The efficiency uncertainty is about 2.5% on average and consists of statistical uncertainties from the *pp* collision dataset and the simulation samples of forward and backward collisions used in the tag-and-probe method, together with the multiplicity weighting uncertainty. Here the multiplicity weighting uncertainty is estimated in the same way as for the background. The FSR correction uncertainty is estimated to be less than 0.1% as the difference of the default correction factors derived using POWHEGBOX with PYTHIA 8 with respect to an alternative approach using PHOTOS [71]. The uncertainty

of the pp reference cross-section at $8.16\,\mathrm{TeV}$ is interpolated to be 0.6% on average as an error band enclosed by the upper and lower edges of the error bars of the 7, 8 and $13\,\mathrm{TeV}$ measurements. The luminosity uncertainty is about 2.5% [37]. For the differential measurements of the cross-section, R_{FB}, and $R_{p\mathrm{Pb}}$ as a function of the p_{T}^{Z}, the detector-resolution correction is applied. The uncertainty is given by the difference between the Bayesian approach and other unfolding techniques [72, 73], which are considered only in the differential measurements.

For the R_{FB} and $R_{p\mathrm{Pb}}$ measurements, uncertainties from the y_{μ}^{*} acceptance corrections k_{FB} and $k_{p\mathrm{Pb}}$ are considered, which include PDF uncertainties, and factorisation and renormalisation scale uncertainties.

The uncertainties of the theoretical predictions shown in the comparisons include the PDF and nPDF uncertainties, and the factorisation and renormalisation scale uncertainties. The (n)PDF uncertainties are estimated by varying the eigenvectors of the (n)PDF sets up and down simultaneously on both the p side and the Pb side. The factorisation and renormalisation scale uncertainties are obtained by varying the scale factors from 0.5 to 2.0. All the theoretical uncertainties are converted to a 68% confidence level when comparing with the measurements.

Table 1 summarises the inputs and their uncertainties for the total cross-section, R_{FB} and $R_{p\mathrm{Pb}}$ measurements. The uncertainties are evaluated separately for R_{FB} and $R_{p\mathrm{Pb}}$ measurements because of the different y_{Z}^{*} coverage between pp, forward and backward $p\mathrm{Pb}$ collisions, and are found to be identical to that for the cross-section measurement.

For the differential measurements of the cross-section, R_{FB}, and $R_{p\mathrm{Pb}}$ as a function of the y_{Z}^{*}, p_{T}^{Z} and ϕ^{*} variables, the uncertainty from the integrated luminosity is considered to be 100% correlated, while the uncertainties from other sources are considered to be partially correlated. Correlation matrices are evaluated for the statistical uncertainty and for the reconstruction and selection efficiency uncertainty, since they form the two largest sources of uncertainty. The statistical uncertainty correlation due to interval migration is evaluated using simulation by comparing the distributions at generator level and reconstruction level. As a result, a $10-26\%$ correlation can be observed for p_{T}^{Z}, a $2-3\%$ correlation for y_{Z}^{*}, and a negligibly small correlation for ϕ^{*}. The correlation matrices for the reconstruction and selection efficiencies are calculated by varying the efficiencies in each interval independently within their uncertainties. Large correlations between different intervals are observed. The resulting correlation matrices for statistical uncertainty and the reconstruction and selection efficiency uncertainties are given in appendix A.

6 Results and discussion

The total fiducial cross-section of $Z \to \mu^{+}\mu^{-}$ production in forward and backward collisions is measured to be

$$\sigma_{Z\to\mu^{+}\mu^{-},\ p\mathrm{Pb}}^{\mathrm{fid}} = 26.9 \pm 1.6 \pm 0.9 \pm 0.7\ \mathrm{nb}\,,$$
$$\sigma_{Z\to\mu^{+}\mu^{-},\ \mathrm{Pb}p}^{\mathrm{fid}} = 13.4 \pm 1.0 \pm 0.5 \pm 0.3\ \mathrm{nb}\,,$$

where the first uncertainty is statistical, the second is systematic and the third is due to the uncertainty in the luminosity determination. As a result of the different muon

rapidity acceptances between forward and backward collisions, the y_Z^* coverage is also different. An additional acceptance requirement of $1.5 < y_Z^* < 4.0$ for forward collisions and $-4.0 < y_Z^* < -2.5$ for backward collisions is applied on top of the fiducial volume.

Figure 2 shows the measured results compared to the POWHEGBOX calculations using the CTEQ6.1 proton PDF set, EPPS16 nPDF and nCTEQ15 nPDF sets. For forward collisions, the measured value agrees with theoretical predictions with a much smaller uncertainty, which indicates a strong constraining power to the theoretical modelling of the nPDFs. For backward collisions, the measured value is slightly higher but statistically compatible with the theory predictions (difference below 2σ). This trend was also observed in the previous result at $\sqrt{s_{\mathrm{NN}}} = 5.02\,\mathrm{TeV}$ [27].

The measured differential fiducial cross-sections as a function of y_Z^* are shown in figure 3 for forward and backward collisions, together with the POWHEGBOX calculations with CTEQ6.1, EPPS16 and nCTEQ15 (n)PDF sets. For forward collisions, the measured values show good agreement with the POWHEGBOX calculations, with a smaller uncertainty for the two intervals of $2.0 < y_Z^* < 3.0$ compared to the theoretical calculations, which can be used to further constrain the nPDFs. For backward collisions, the uncertainty of the measurement is larger than that of the POWHEGBOX calculation, and the measured central value is higher than the prediction especially for the $-3.5 < y_Z^* < -3.0$ interval by about 2σ. However, the measurement and calculation are compatible within uncertainties.

The differential fiducial cross-section as a function of p_{T}^Z is shown in figure 4 (a) and (b), together with the POWHEGBOX calculations. For forward collisions, the measured values give a smaller uncertainty compared to the POWHEGBOX calculation for low p_{T}^Z intervals, showing a strong constraining power. For backward collisions, the uncertainty of the measurement is larger than that of the POWHEGBOX calculations but statistically compatible. For p_{T}^Z above $30\,\mathrm{GeV}$ the central value of the measurement is slightly larger than the POWHEGBOX calculations, but statistically compatible with them for both forward and backward collisions. The same cross-section measurement as a function of p_{T}^Z at low transverse momentum, where non-perturbation effects start to dominate, is also provided with finer intervals, in order to aid theoretical TMD studies, as shown in figure 4 (c) and (d). The differential fiducial cross-section as a function of the ϕ^* variable is shown in figure 5 together with the POWHEGBOX calculations. Since the angular observable ϕ^* is equivalent to p_{T}^Z but not impacted by the momentum resolution, a similar conclusion can be drawn as for p_{T}^Z. The detailed numerical values and uncertainties of the differential cross-section as a function of y_Z^*, p_{T}^Z and ϕ^*, together with the corresponding f_{FSR} factors are given in appendix B.

The cross-sections used to determine the forward-backward ratio are different with respect to the fiducial cross-sections. They are measured in the common Z-boson rapidity range $2.5 < |y_Z^*| < 4.0$ with efficiency, purity and FSR corrections also determined in the same rapidity range as shown in table 1, These corrections are found to be identical to those of the fiducial cross-section measurement. The resulting cross-sections for R_{FB} measurements are $16.1 \pm 1.5\,\mathrm{nb}$ and $13.4 \pm 1.2\,\mathrm{nb}$ for forward and backward collisions, respectively. To eliminate the impact from different y_μ^* acceptances, the correction factor k_{FB} for the overall R_{FB} measurement is calculated to be 0.65 ± 0.02.
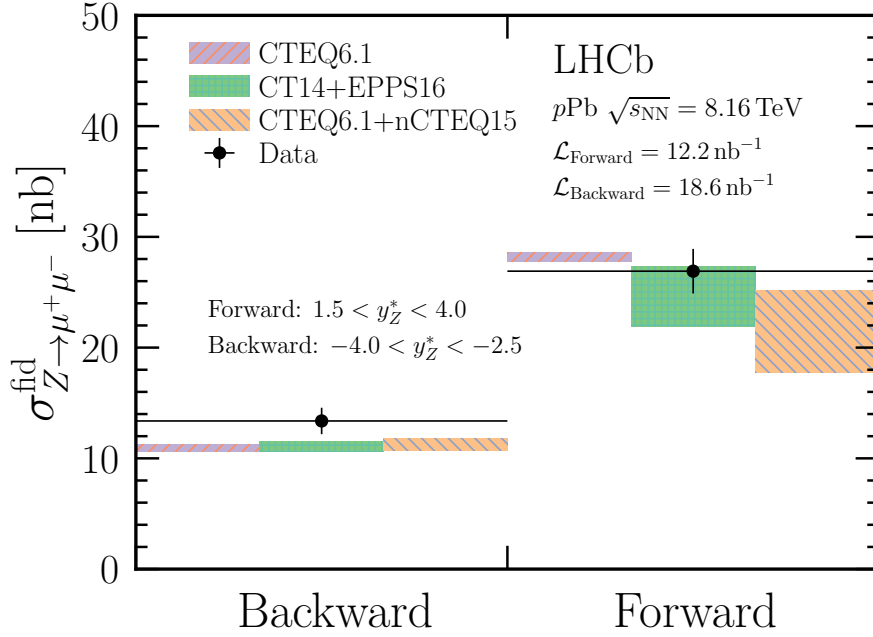
Figure 2. The measured overall $Z \to \mu^+\mu^-$ production fiducial cross-section compared to the PowhegBox prediction using CTEQ6.1, EPPS16 and nCTEQ15 (n)PDF sets, for forward and backward collisions, respectively.
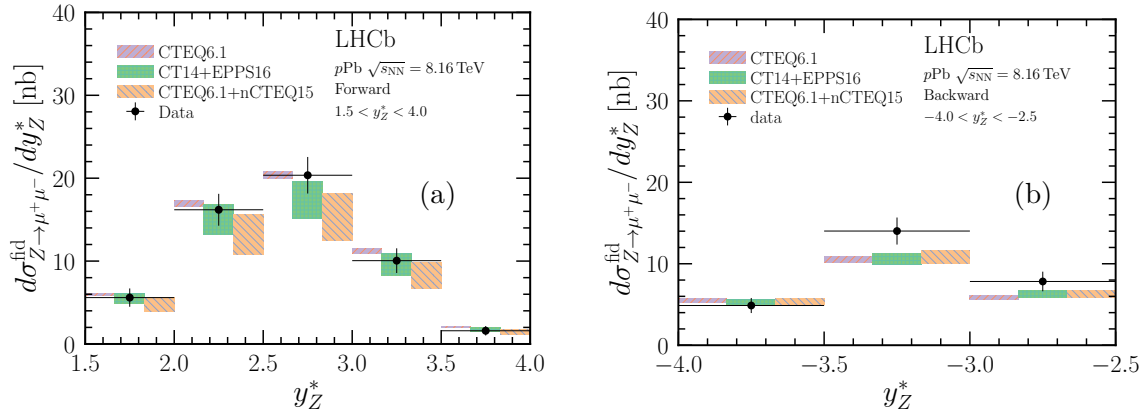
Figure 3. The measured differential fiducial cross-section as a function of y_Z^* for (a) forward and (b) backward collisions. The theoretical predictions are calculated using PowhegBox with CTEQ6.1, EPPS16 and nCTEQ15 (n)PDF sets.
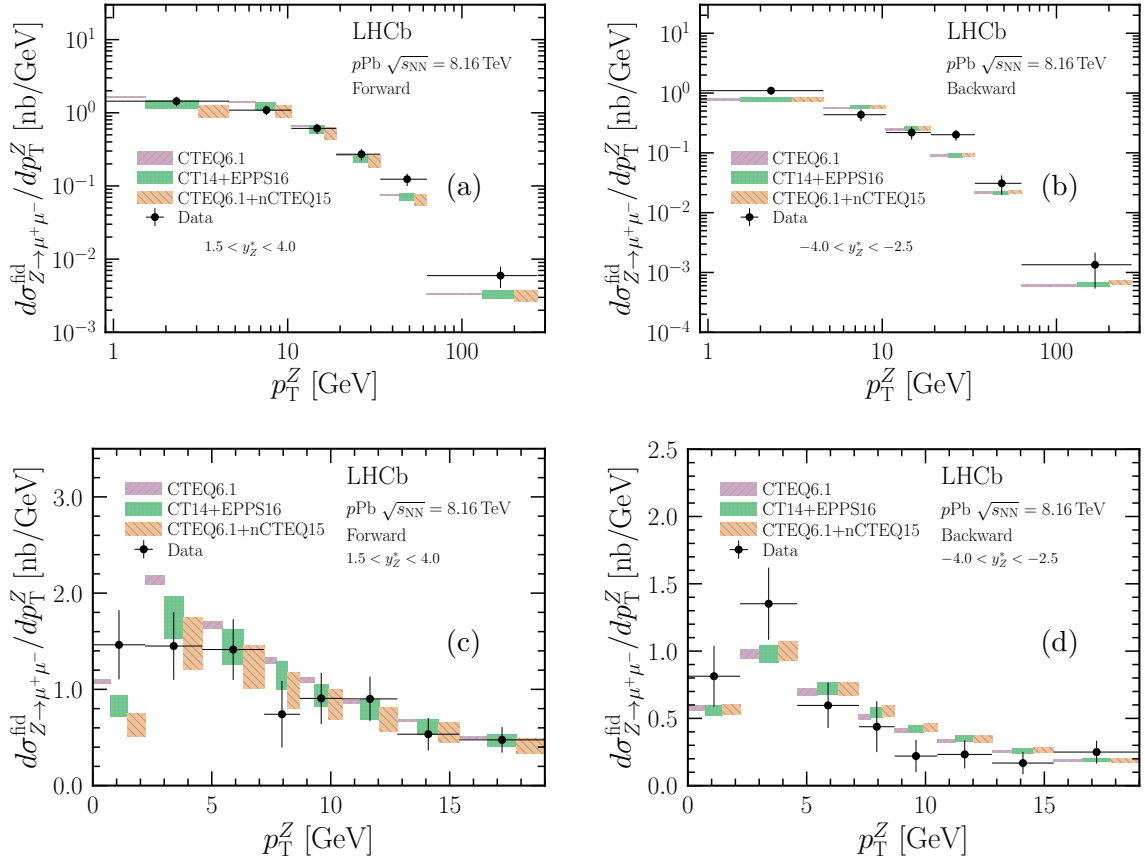
Figure 4. The measured differential fiducial cross-section as a function of p_T^Z for (a) forward and (b) backward collisions, and the corresponding version for (c) forward and (d) backward collisions with fine intervals at low p_T^Z. The theoretical predictions are calculated using PowhegBox with CTEQ6.1, EPPS16 and nCTEQ15 (n)PDF sets.
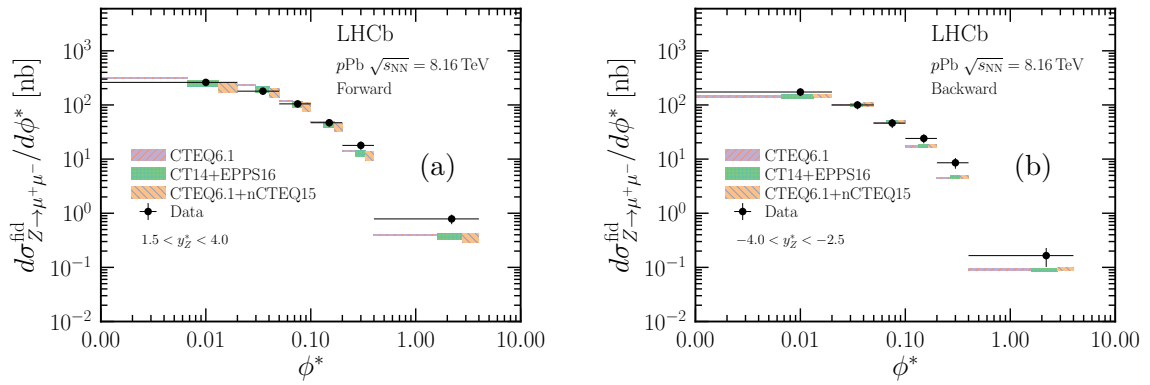
Figure 5. The measured differential fiducial cross-section as a function of ϕ^* for (a) forward and (b) backward collisions. The theoretical predictions are calculated using PowhegBox with CTEQ6.1, EPPS16 and nCTEQ15 (n)PDF sets.

y_Z^*	$[2.5, 3.0]$	$[3.0, 3.5]$	$[3.5, 4.0]$			
$k_{\text{FB}}(y_Z^*)$	0.29 ± 0.01	0.94 ± 0.04	2.73 ± 0.13			
p_{T}^Z [GeV]	$[0, 4.6]$	$[4.6, 10.5]$	$[10.5, 19]$	$[19, 34]$	$[34, 63]$	$[63, 270]$
$k_{\text{FB}}(p_{\text{T}}^Z)$	0.72 ± 0.03	0.65 ± 0.03	0.63 ± 0.03	0.59 ± 0.03	0.58 ± 0.02	0.46 ± 0.02
ϕ^*	$[0, 0.02]$	$[0.02, 0.05]$	$[0.05, 0.1]$	$[0.1, 0.2]$	$[0.2, 0.4]$	$[0.4, 4]$
$k_{\text{FB}}(\phi^*)$	0.70 ± 0.03	0.67 ± 0.03	0.65 ± 0.03	0.62 ± 0.03	0.59 ± 0.03	0.49 ± 0.02

Table 2. The y_μ^* acceptance correction factors (k_{FB}) for R_{FB} measured in intervals of y_Z^*, p_{T}^Z, and ϕ^*.

The value of R_{FB} is then measured to be $R_{\text{FB}} = 0.78 \pm 0.10$, as shown in figure 6. The measured R_{FB} value is below unity, which is a reflection of the suppression due to, *e.g.*, nuclear shadowing at small Bjorken-x, together with an average enhancement at large Bjorken-x. The data is in agreement with the EPPS16 and nCTEQ15 predictions. The uncertainty of the measurement is smaller than the theoretical uncertainties using EPPS16 and nCTEQ15 nPDFs, which shows a constraining power on the nPDFs.

In addition, the value of R_{FB} is also measured differentially as a function of y_Z^*, p_{T}^Z and ϕ^*. The corresponding k_{FB} correction factors for the differential measurements are derived in the same way in separate intervals as shown in table 2. Figure 6 (b), (c), and (d) show the above measured values of R_{FB} as a function of y_Z^*, p_{T}^Z and ϕ^*, respectively, together with the theory calculations. The R_{FB} measurement as a function of y_Z^* shows a general suppression below unity for all three intervals, in good agreement with the nPDF predictions. For the two intervals in $2.5 < y_Z^* < 3.5$ the measurements give a smaller uncertainty compared to the nCTEQ15 prediction which can be used to constrain the nPDFs. For the R_{FB} measurements as a function of p_{T}^Z and ϕ^*, a general suppression is expected, however, the significance of the suppression is weak given the large statistical fluctuation in the differential measurements. From theory a slightly stronger suppression at lower p_{T}^Z or ϕ^* is expected, but given the precision of the current measurement this tendency is not visible. The R_{FB} as a function of ϕ^* shows a more stable trend than as a function of p_{T}^Z, which exhibits a larger fluctuation The detailed numerical values and uncertainties of the differential measurements of the R_{FB} together with the corresponding f_{FSR} factors are given in appendix B.

For the total nuclear modification factor measurements, because the y_Z^* coverage between pp and pPb collisions is different, the common y_Z^* acceptance range $2.0 < y_Z^* < 4.0$ for forward rapidity and $-4.0 < y_Z^* < -2.5$ for backward rapidity is used. The y_μ^* acceptance correction factors are determined to be $k_{p\text{Pb}}^{\text{fw}} = 0.706 \pm 0.002$ and $k_{p\text{Pb}}^{\text{bw}} = 1.518 \pm 0.003$ for forward and backward rapidities, respectively. The cross-sections to be used in the $R_{p\text{Pb}}$ calculations are measured to be 24.2 ± 1.9 nb and 13.4 ± 1.2 nb for forward and backward collisions, respectively, in the corresponding y_Z^* common acceptance ranges. The variables required to calculate these cross-sections are shown in table 1. The corresponding pp reference cross-sections at 8.16 TeV are interpolated in the corresponding y_Z^* common acceptance ranges as $(95.18 \pm 0.55) \times 10^{-3}$ nb and $(79.10 \pm 0.51) \times 10^{-3}$ nb for forward and backward rapidities, respectively.
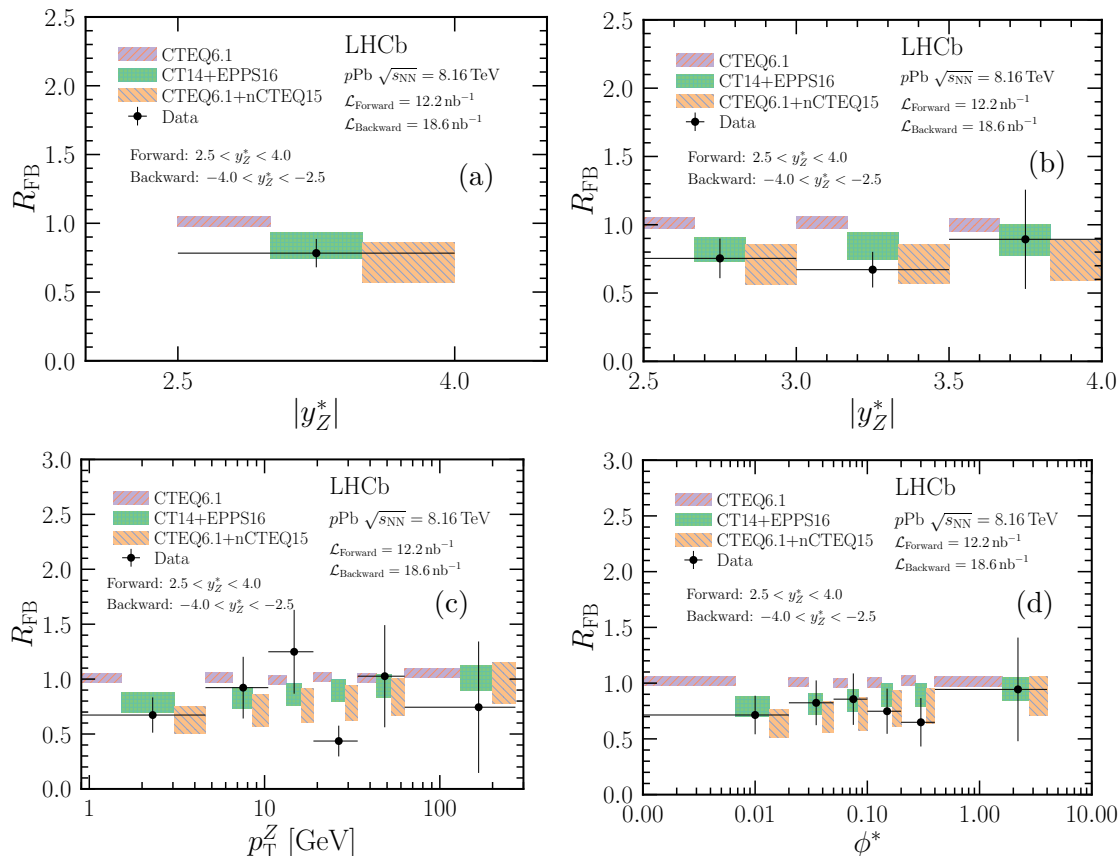
Figure 6. The measured forward-backward ratio (R_{FB}), (a) for the overall measurement, (b) as a function of y_Z^*, (c) as a function of p_T^Z, and (d) as a function of ϕ^*, together with the PowhegBox predictions using CTEQ6.1, EPPS16 and nCTEQ15 (n)PDF sets.

The measured overall nuclear modification factors are $R_{p\text{Pb}}^{\text{fw}} = 0.94 \pm 0.07$ and $R_{p\text{Pb}}^{\text{bw}} = 1.20 \pm 0.11$ for forward and backward rapidities, respectively, where the total uncertainties are given. These results are shown in figure 7 compared with the PowhegBox predictions using the EPPS16 and nCTEQ15 nPDF sets. The overall $R_{p\text{Pb}}$ results show good compatibility between measurements and theoretical predictions. The backward rapidity result shows larger uncertainty compared to that of the nPDF sets. The measured central value is consistent with the prediction at a 2σ level. The forward rapidity result gives a higher precision than the EPPS16 and nCTEQ15 nPDF sets, and the central value is larger than the prediction, which shows a constraining power on the current nPDF sets.

For the differential measurements of the $R_{p\text{Pb}}$, the forward and backward cross-sections and the corresponding pp reference cross-sections are determined in the same way as for the total $R_{p\text{Pb}}$ measurement but in intervals of y_Z^*, p_T^Z and ϕ^*. The y_μ^* acceptance correction factors $k_{p\text{Pb}}$ for the differential measurements are also derived using PowhegBox with the CTEQ6.1 PDF set considering theory uncertainties from PDF variations and the factorisation and renormalisation scales, as shown in table 3. The resulting $R_{p\text{Pb}}$ values as a function of y_Z^*, p_T^Z and ϕ^* are shown in figure 8. In general these results are compatible
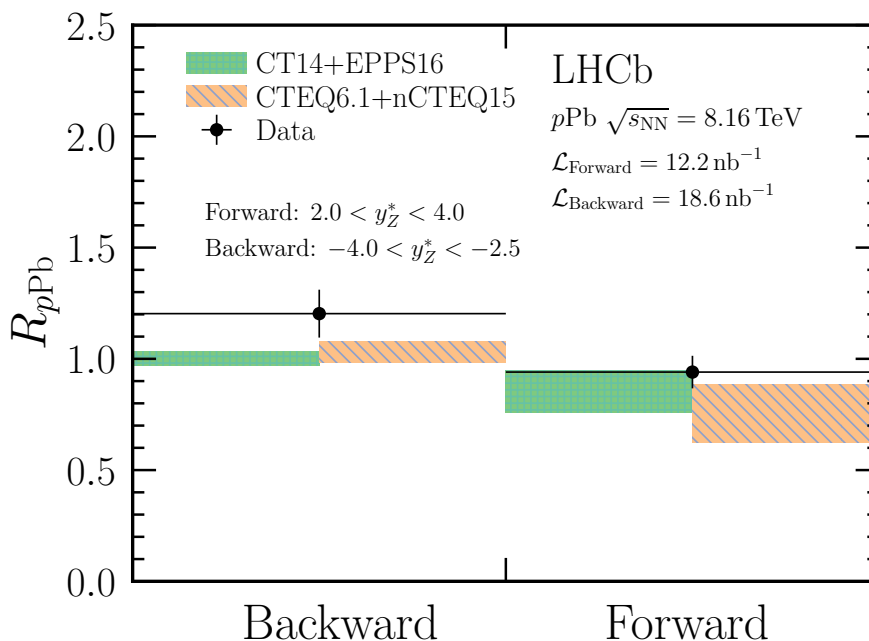
Figure 7. Measurements of the nuclear modification factor ($R_{p\mathrm{Pb}}$) compared to the PowhegBox predictions using the EPPS16 and nCTEQ15 (n)PDF sets.

		y_Z^*	[2.0, 2.5]	[2.5, 3.0]	[3.0, 3.5]	[3.5, 4.0]		
$k_{p\mathrm{Pb}}$ (y_Z^*)	forward		0.3713	0.7468	1.2482	2.1875		
			±0.0005	±0.0004	±0.0010	±0.0004		
		y_Z^*	[−4.0, −3.5]	[−3.5, −3.0]	[−3.0, −2.5]			
$k_{p\mathrm{Pb}}$ (y_Z^*)	backward		0.7935	1.3177	2.5525			
			±0.0001	±0.0001	±0.0009			
		p_T^Z [GeV]	[0, 4.6]	[4.6, 10.5]	[10.5, 19]	[19, 34]	[34, 63]	[63, 270]
$k_{p\mathrm{Pb}}$ (p_T^Z)	forward		0.7821	0.7212	0.6903	0.6613	0.6136	0.5455
			±0.0056	±0.0049	±0.0045	±0.0040	±0.0035	±0.0027
	backward		1.6073	1.7735	1.8341	1.9387	2.0742	2.8031
			±0.0034	±0.0039	±0.0040	±0.0045	±0.0047	±0.0069
		ϕ^*	[0, 0.02]	[0.02, 0.05]	[0.05, 0.1]	[0.1, 0.2]	[0.2, 0.4]	[0.4, 4]
$k_{p\mathrm{Pb}}$ (ϕ^*)	forward		0.7702	0.7322	0.7080	0.6804	0.6461	0.5756
			±0.0054	±0.0049	±0.0047	±0.0043	±0.0040	±0.0032
	backward		1.6400	1.7113	1.8105	1.8645	1.9741	2.4238
			±0.0036	±0.0036	±0.0041	±0.043	±0.0047	±0.0065

Table 3. The y_μ^* acceptance correction factors ($k_{p\mathrm{Pb}}$) for $R_{p\mathrm{Pb}}$ measured in intervals of y_Z^*, p_T^Z, and ϕ^* for forward and backward collisions.

with nPDF predictions. For backward rapidity, larger uncertainties compared to the current nPDF predictions appear for all three observables. However, for forward rapidity the larger dataset gives a higher precision for certain intervals compared to the nPDF predictions. The detailed numerical values and uncertainties of the $R_{p\mathrm{Pb}}$ as a function of y_Z^*, p_T^Z, and ϕ^*, together with the corresponding f_{FSR} factors are given in appendix B.
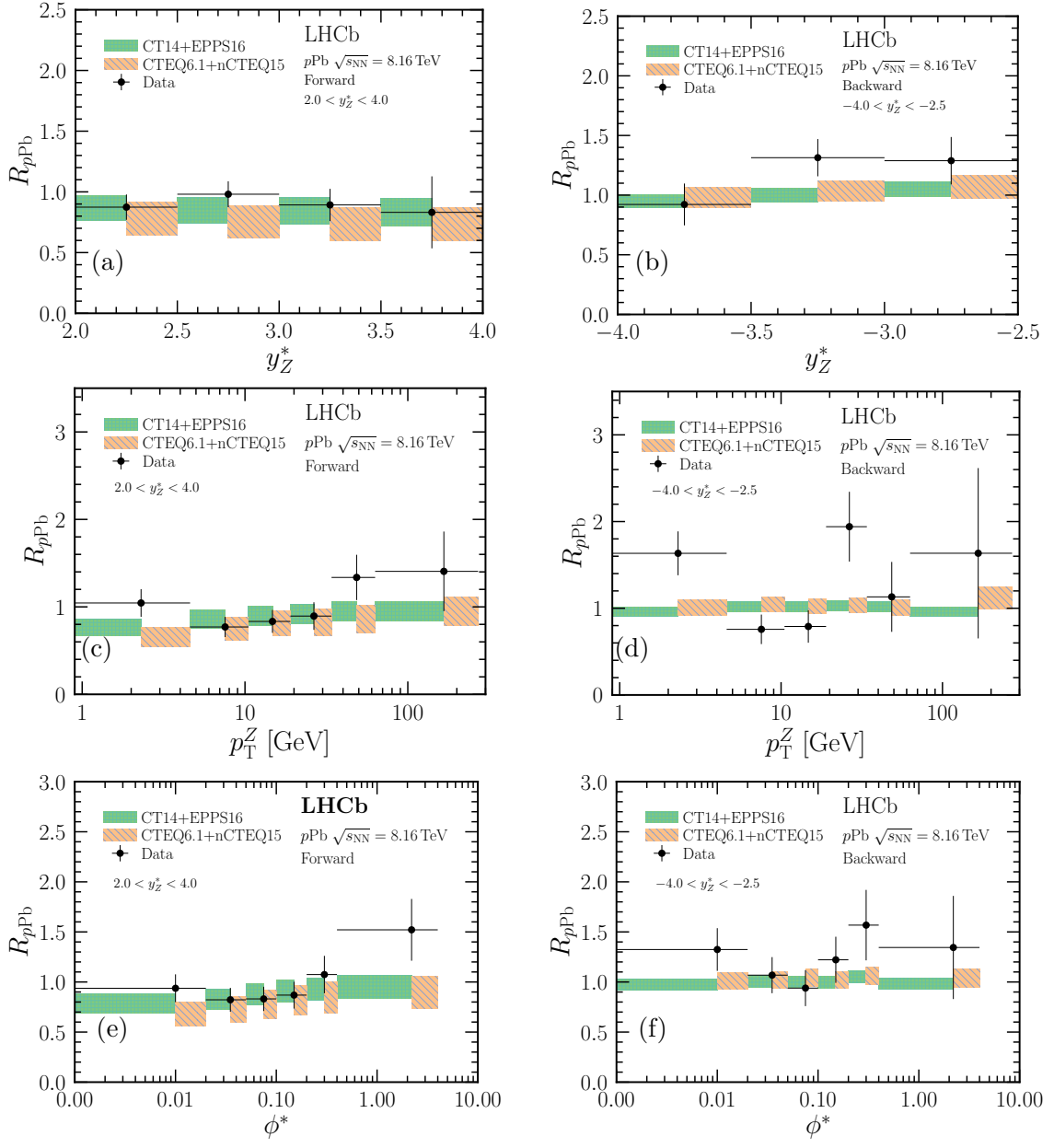
Figure 8. Nuclear modification factors ($R_{p\mathrm{Pb}}$) as a function of (top row) y_Z^*, (middle row) p_T^Z and (bottom row) ϕ^*, together with the PowhegBox prediction using EPPS16 and nCTEQ15 nPDF sets, where the left column is for forward collisions and the right column is for backward collisions.

7 Conclusion

This article presents a comprehensive analysis of $Z \to \mu^+\mu^-$ production using pPb collisions at 8.16 TeV in the forward region recorded with the LHCb detector. The Z-boson production fiducial cross-section, R_{FB} and $R_{p\mathrm{Pb}}$ are measured inclusively and differentially as a function of y_Z^*, p_{T}^Z, and ϕ^*. The results are compatible with theoretical predictions from the EPPS16 and nCTEQ15 nPDFs. The precision of the measurements is significantly improved compared to the previous LHCb results using pPb collisions at a centre-of-mass energy of 5.02 TeV [27] collected in 2013. The measurements provide strong constraints on the nPDFs, especially at high rapidity corresponding to the small Bjorken-x region from 10^{-4} to 10^{-3}.

A   Statistical and systematic correlation matrices

y_Z^*	Index	1	2	3	4	5
$[1.5, 2.0]$	1	1.00				
$[2.0, 2.5]$	2	0.01	1.00			
$[2.5, 3.0]$	3	0.00	0.01	1.00		
$[3.0, 3.5]$	4	0.00	0.00	0.01	1.00	
$[3.5, 4.0]$	5	0.00	0.00	0.00	0.00	1.00

Table 4. Correlation matrix of statistical uncertainty in y_Z^* intervals for forward collisions.

y_Z^*	Index	1	2	3
$[-3.0, -2.5]$	1	1.00		
$[-3.5, -3.0]$	2	0.01	1.00	
$[-4.0, -3.5]$	3	0.00	0.01	1.00

Table 5. Correlation matrix of statistical uncertainty in y_Z^* intervals for backward collisions.

p_T^Z [GeV]	Index	1	2	3	4	5	6
$[0.0, 4.6]$	1	1.00					
$[4.6, 10.5]$	2	0.93	1.00				
$[10.5, 19.0]$	3	0.00	0.05	1.00			
$[19.0, 34.0]$	4	0.00	0.00	0.04	1.00		
$[34.0, 63.0]$	5	0.00	0.00	0.00	0.03	1.00	
$[63.0, 270.0]$	6	0.00	0.00	0.00	0.00	0.02	1.00

Table 6. Correlation matrix of statistical uncertainty in p_T^Z intervals for forward collisions.

p_T^Z [GeV]	Index	1	2	3	4	5	6
$[0.0, 4.6]$	1	1.00					
$[4.6, 10.5]$	2	0.08	1.00				
$[10.5, 19.0]$	3	0.00	0.04	1.00			
$[19.0, 34.0]$	4	0.00	0.00	0.03	1.00		
$[34.0, 63.0]$	5	0.00	0.00	0.00	0.02	1.00	
$[63.0, 270.0]$	6	0.00	0.00	0.00	0.00	0.01	1.00

Table 7. Correlation matrix of statistical uncertainty in p_T^Z intervals for backward collisions.

ϕ^*	Index	1	2	3	4	5	6
[0.00, 0.02]	1	1.00					
[0.02, 0.05]	2	0.01	1.00				
[0.05, 0.10]	3	0.00	0.00	1.00			
[0.10, 0.20]	4	0.00	0.00	0.00	1.00		
[0.20, 0.40]	5	0.00	0.00	0.00	0.00	1.00	
[0.40, 4.00]	6	0.00	0.00	0.00	0.00	0.00	1.00

Table 8. Correlation matrix of statistical uncertainty in ϕ^* intervals for forward collisions.

ϕ^*	Index	1	2	3	4	5	6
[0.00, 0.02]	1	1.00					
[0.02, 0.05]	2	0.00	1.00				
[0.05, 0.10]	3	0.00	0.00	1.00			
[0.10, 0.20]	4	0.00	0.00	0.00	1.00		
[0.20, 0.40]	5	0.00	0.00	0.00	0.00	1.00	
[0.40, 4.00]	6	0.00	0.00	0.00	0.00	0.00	1.00

Table 9. Correlation matrix of statistical uncertainty in ϕ^* intervals for backward collisions.

p_{T}^Z [GeV]	Index	1	2	3	4	5	6	7	8
[0.0, 2.2]	1	1.00							
[2.2, 4.6]	2	0.24	1.00						
[4.6, 7.2]	3	0.04	0.26	1.00					
[7.2, 8.7]	4	0.01	0.04	0.25	1.00				
[8.7, 10.5]	5	0.01	0.01	0.04	0.24	1.00			
[10.5, 12.8]	6	0.00	0.01	0.01	0.03	0.21	1.00		
[12.8, 15.4]	7	0.00	0.00	0.01	0.01	0.03	0.20	1.00	
[15.4, 19.0]	8	0.00	0.00	0.00	0.01	0.01	0.02	0.18	1.00

Table 10. Correlation matrix of statistical uncertainty in p_{T}^Z intervals for forward collisions in the low p_{T}^Z range.

p_{T}^Z [GeV]	Index	1	2	3	4	5	6	7	8
[0.0, 2.2]	1	1.00							
[2.2, 4.6]	2	0.20	1.00						
[4.6, 7.2]	3	0.03	0.22	1.00					
[7.2, 8.7]	4	0.01	0.03	0.21	1.00				
[8.7, 10.5]	5	0.01	0.01	0.02	0.20	1.00			
[10.5, 12.8]	6	0.00	0.00	0.01	0.02	0.18	1.00		
[12.8, 15.4]	7	0.00	0.00	0.00	0.01	0.02	0.17	1.00	
[15.4, 19.0]	8	0.00	0.00	0.00	0.00	0.01	0.02	0.14	1.00

Table 11. Correlation matrix of statistical uncertainty in p_{T}^Z intervals for backward collisions in the low p_{T}^Z range.

y_Z^*	Index	1	2	3	4	5
$[2.0, 2.5]$	1	1.00				
$[2.5, 3.0]$	2	0.71	1.00			
$[3.0, 3.5]$	3	0.37	0.72	1.00		
$[3.5, 4.0]$	4	0.03	0.24	0.71	1.00	
$[4.0, 4.5]$	5	0.00	0.05	0.45	0.79	1.00

Table 12. Correlation matrix of efficiency uncertainty in y_Z^* intervals for forward collisions.

y_Z^*	Index	1	2	3
$[-3.0, -2.5]$	1	1.00		
$[-3.5, -3.0]$	2	0.64	1.00	
$[-4.0, -3.5]$	3	0.48	0.75	1.00

Table 13. Correlation matrix of efficiency uncertainty in y_Z^* intervals for backward collisions.

p_T^Z [GeV]	Index	1	2	3	4	5	6
$[0.0, 4.6]$	1	1.00					
$[4.6, 10.5]$	2	0.88	1.00				
$[10.5, 19.0]$	3	0.87	0.89	1.00			
$[19.0, 34.0]$	4	0.92	0.89	0.91	1.00		
$[34.0, 63.0]$	5	0.85	0.80	0.79	0.87	1.00	
$[63.0, 270.0]$	6	0.75	0.82	0.82	0.82	0.74	1.00

Table 14. Correlation matrix of efficiency uncertainty in p_T^Z intervals for forward collisions.

p_T^Z [GeV]	Index	1	2	3	4	5	6
$[0.0, 4.6]$	1	1.00					
$[4.6, 10.5]$	2	0.85	1.00				
$[10.5, 19.0]$	3	0.91	0.91	1.00			
$[19.0, 34.0]$	4	0.83	0.94	0.86	1.00		
$[34.0, 63.0]$	5	0.68	0.84	0.65	0.80	1.00	
$[63.0, 270.0]$	6	0.50	0.71	0.65	0.70	0.77	1.00

Table 15. Correlation matrix of efficiency uncertainty in p_T^Z intervals for backward collisions.

ϕ^*	Index	1	2	3	4	5	6
$[0.00, 0.02]$	1	1.00					
$[0.02, 0.05]$	2	0.83	1.00				
$[0.05, 0.10]$	3	0.92	0.90	1.00			
$[0.10, 0.20]$	4	0.83	0.85	0.80	1.00		
$[0.20, 0.40]$	5	0.85	0.71	0.77	0.73	1.00	
$[0.40, 4.00]$	6	0.85	0.89	0.85	0.81	0.82	1.00

Table 16. Correlation matrix of efficiency uncertainty in ϕ^* intervals for forward collisions.

ϕ^*	Index	1	2	3	4	5	6
[0.00, 0.02]	1	1.00					
[0.02, 0.05]	2	0.90	1.00				
[0.05, 0.10]	3	0.88	0.80	1.00			
[0.10, 0.20]	4	0.80	0.79	0.77	1.00		
[0.20, 0.40]	5	0.76	0.70	0.79	0.58	1.00	
[0.40, 4.00]	6	0.53	0.60	0.55	0.75	0.54	1.00

Table 17. Correlation matrix of efficiency uncertainty in ϕ^* intervals for backward collisions.

p_T^Z [GeV]	Index	1	2	3	4	5	6	7	8
[0.0, 2.2]	1	1.00							
[2.2, 4.6]	2	0.57	1.00						
[4.6, 7.2]	3	0.71	0.83	1.00					
[7.2, 8.7]	4	0.57	0.67	0.68	1.00				
[8.7, 10.5]	5	0.61	0.71	0.80	0.68	1.00			
[10.5, 12.8]	6	0.72	0.73	0.83	0.64	0.85	1.00		
[12.8, 15.4]	7	0.66	0.77	0.84	0.62	0.71	0.85	1.00	
[15.4, 19.0]	8	0.58	0.78	0.78	0.46	0.76	0.77	0.70	1.00

Table 18. Correlation matrix of efficiency uncertainty in p_T^Z intervals for forward collisions in the low p_T^Z range.

p_T^Z [GeV]	Index	1	2	3	4	5	6	7	8
[0.0, 2.2]	1	1.00							
[2.2, 4.6]	2	0.82	1.00						
[4.6, 7.2]	3	0.73	0.76	1.00					
[7.2, 8.7]	4	0.78	0.66	0.70	1.00				
[8.7, 10.5]	5	0.48	0.74	0.58	0.48	1.00			
[10.5, 12.8]	6	0.86	0.84	0.69	0.61	0.58	1.00		
[12.8, 15.4]	7	0.72	0.72	0.67	0.88	0.55	0.52	1.00	
[15.4, 19.0]	8	0.79	0.78	0.81	0.81	0.55	0.74	0.71	1.00

Table 19. Correlation matrix of efficiency uncertainty in p_T^Z intervals for backward collisions in the low p_T^Z range.

B Differential cross-section, forward-backward ratio, and nuclear modification factors

	y_Z^*	$d\sigma/dy_Z^*$ [nb]	f_{FSR}
Forward	$[1.5, 2.0]$	$5.60 \pm 1.08 \pm 0.20 \pm 0.15$	1.017 ± 0.002
	$[2.0, 2.5]$	$16.19 \pm 1.80 \pm 0.53 \pm 0.43$	1.020 ± 0.001
	$[2.5, 3.0]$	$20.36 \pm 2.02 \pm 0.72 \pm 0.53$	1.023 ± 0.001
	$[3.0, 3.5]$	$10.05 \pm 1.42 \pm 0.36 \pm 0.26$	1.030 ± 0.001
	$[3.5, 4.0]$	$1.59 \pm 0.56 \pm 0.06 \pm 0.04$	1.014 ± 0.002
Backward	$[-4.0, -3.5]$	$4.87 \pm 0.89 \pm 0.17 \pm 0.18$	1.028 ± 0.002
	$[-3.5, -3.0]$	$14.02 \pm 1.49 \pm 0.49 \pm 0.53$	1.018 ± 0.001
	$[-3.0, -2.5]$	$7.83 \pm 1.13 \pm 0.30 \pm 0.30$	1.020 ± 0.001

Table 20. Differential cross-section of $Z \to \mu^+\mu^-$ in intervals of y_Z^* for forward and backward collisions, together with the FSR correction. In the differential cross-section results, the first uncertainty is statistical, the second is systematic and the third is from integrated luminosity.

	p_{T}^Z [GeV]	$d\sigma/dp_{\mathrm{T}}^Z$ [nb/ GeV]	f_{FSR}
Forward	$[0.0, 4.6]$	$1.441 \pm 0.209 \pm 0.046 \pm 0.038$	1.068 ± 0.002
	$[4.6, 10.5]$	$1.086 \pm 0.156 \pm 0.035 \pm 0.029$	1.033 ± 0.001
	$[10.5, 19.0]$	$0.612 \pm 0.092 \pm 0.020 \pm 0.016$	0.994 ± 0.002
	$[19.0, 34.0]$	$0.272 \pm 0.046 \pm 0.010 \pm 0.007$	0.988 ± 0.002
	$[34.0, 63.0]$	$0.124 \pm 0.023 \pm 0.005 \pm 0.003$	1.034 ± 0.002
	$[63.0, 270.0]$	$(5.9 \pm 1.9 \pm 0.4 \pm 0.2) \times 10^{-3}$	1.043 ± 0.007
Backward	$[0.0, 4.6]$	$1.097 \pm 0.162 \pm 0.042 \pm 0.027$	1.082 ± 0.002
	$[4.6, 10.5]$	$0.434 \pm 0.096 \pm 0.016 \pm 0.011$	1.025 ± 0.002
	$[10.5, 19.0]$	$0.218 \pm 0.051 \pm 0.009 \pm 0.005$	0.976 ± 0.002
	$[19.0, 34.0]$	$0.201 \pm 0.040 \pm 0.009 \pm 0.005$	0.981 ± 0.002
	$[34.0, 63.0]$	$0.031 \pm 0.011 \pm 0.002 \pm 0.001$	1.028 ± 0.003
	$[63.0, 270.0]$	$(1.3 \pm 0.8 \pm 0.1 \pm 0.1) \times 10^{-3}$	1.064 ± 0.009

Table 21. Differential cross-section of $Z \to \mu^+\mu^-$ in intervals of p_{T}^Z for forward and backward collisions, together with the FSR correction. In the differential cross-section results, the first uncertainty is statistical, the second is systematic and the third is from integrated luminosity.

	p_{T}^{Z} [GeV]	$d\sigma/dp_{\mathrm{T}}^{Z}$ [nb/ GeV]	f_{FSR}
Forward	[0.0, 2.2]	$1.463 \pm 0.352 \pm 0.059 \pm 0.038$	1.079 ± 0.002
	[2.2, 4.6]	$1.450 \pm 0.347 \pm 0.045 \pm 0.038$	1.064 ± 0.002
	[4.6, 7.2]	$1.414 \pm 0.310 \pm 0.044 \pm 0.037$	1.048 ± 0.004
	[7.2, 8.7]	$0.742 \pm 0.344 \pm 0.027 \pm 0.019$	1.035 ± 0.004
	[8.7, 10.5]	$0.906 \pm 0.261 \pm 0.044 \pm 0.024$	1.005 ± 0.002
	[10.5, 12.8]	$0.901 \pm 0.227 \pm 0.037 \pm 0.024$	1.003 ± 0.003
	[12.8, 15.4]	$0.534 \pm 0.167 \pm 0.020 \pm 0.014$	1.000 ± 0.004
	[15.4, 19.0]	$0.475 \pm 0.130 \pm 0.022 \pm 0.012$	0.981 ± 0.002
Backward	[0.0, 2.2]	$0.813 \pm 0.223 \pm 0.029 \pm 0.020$	1.107 ± 0.004
	[2.2, 4.6]	$1.352 \pm 0.259 \pm 0.062 \pm 0.033$	1.072 ± 0.004
	[4.6, 7.2]	$0.596 \pm 0.166 \pm 0.024 \pm 0.015$	1.037 ± 0.006
	[7.2, 8.7]	$0.438 \pm 0.187 \pm 0.024 \pm 0.011$	1.025 ± 0.003
	[8.7, 10.5]	$0.220 \pm 0.119 \pm 0.011 \pm 0.005$	0.999 ± 0.003
	[10.5, 12.8]	$0.232 \pm 0.104 \pm 0.008 \pm 0.006$	0.991 ± 0.004
	[12.8, 15.4]	$0.168 \pm 0.083 \pm 0.008 \pm 0.004$	0.965 ± 0.006
	[15.4, 19.0]	$0.250 \pm 0.083 \pm 0.012 \pm 0.006$	0.970 ± 0.004

Table 22. Differential cross-section of $Z \to \mu^+\mu^-$ in intervals of p_{T}^{Z} for forward and backward collisions in the low p_{T}^{Z} region, together with the FSR correction. In the differential cross-section results, the first uncertainty is statistical, the second is systematic and the third is from integrated luminosity.

	ϕ^*	$d\sigma/d\phi^*$ [nb]	f_{FSR}
Forward	[0.0, 0.0]	$261.288 \pm 36.234 \pm 10.959 \pm 6.865$	1.031 ± 0.003
	[0.0, 0.1]	$179.805 \pm 24.698 \pm 6.125 \pm 4.724$	1.044 ± 0.002
	[0.1, 0.1]	$104.654 \pm 14.375 \pm 3.886 \pm 2.750$	1.010 ± 0.002
	[0.1, 0.2]	$46.938 \pm 6.847 \pm 1.765 \pm 1.233$	1.018 ± 0.001
	[0.2, 0.4]	$17.902 \pm 2.984 \pm 0.656 \pm 0.470$	1.004 ± 0.002
	[0.4, 4.0]	$0.786 \pm 0.151 \pm 0.042 \pm 0.021$	1.024 ± 0.004
Backward	[0.0, 0.0]	$173.372 \pm 26.752 \pm 6.029 \pm 4.292$	1.053 ± 0.003
	[0.0, 0.1]	$99.962 \pm 16.216 \pm 3.547 \pm 2.475$	1.007 ± 0.002
	[0.1, 0.1]	$46.233 \pm 8.585 \pm 1.672 \pm 1.145$	1.015 ± 0.002
	[0.1, 0.2]	$24.080 \pm 4.396 \pm 0.863 \pm 0.596$	1.014 ± 0.001
	[0.2, 0.4]	$8.552 \pm 1.866 \pm 0.355 \pm 0.212$	1.015 ± 0.002
	[0.4, 4.0]	$0.165 \pm 0.062 \pm 0.009 \pm 0.004$	1.023 ± 0.004

Table 23. Differential cross-section of $Z \to \mu^+\mu^-$ in intervals of ϕ^* for forward and backward collisions, together with the FSR correction. In the differential cross-section results, the first uncertainty is statistical, the second is systematic and the third is from integrated luminosity.

$|y_Z^*|$	R_{FB}	f_{FSR} (forward)	f_{FSR} (backward)
$[2.5, 3.0]$	$0.75 \pm 0.13 \pm 0.27 \pm 0.26$	1.023 ± 0.001	1.020 ± 0.001
$[3.0, 3.5]$	$0.67 \pm 0.12 \pm 0.24 \pm 0.24$	1.030 ± 0.001	1.018 ± 0.001
$[3.5, 4.0]$	$0.89 \pm 0.36 \pm 0.71 \pm 0.71$	1.014 ± 0.002	1.028 ± 0.002

Table 24. The forward-backward ratio (R_{FB}) in intervals of $|y_Z^*|$, together with the FSR correction. For the R_{FB} results, the first uncertainty is statistical, the second is systematic and the third is from integrated luminosity.

p_{T}^Z [GeV]	R_{FB}	f_{FSR} (forward)	f_{FSR} (backward)
$[0.0, 4.6]$	$0.67 \pm 0.15 \pm 0.04 \pm 0.02$	1.068 ± 0.002	1.082 ± 0.002
$[4.6, 10.5]$	$0.92 \pm 0.27 \pm 0.06 \pm 0.03$	1.033 ± 0.001	1.025 ± 0.002
$[10.5, 19.0]$	$1.25 \pm 0.37 \pm 0.08 \pm 0.05$	0.994 ± 0.002	0.976 ± 0.002
$[19.0, 34.0]$	$0.44 \pm 0.14 \pm 0.03 \pm 0.02$	0.988 ± 0.002	0.981 ± 0.002
$[34.0, 63.0]$	$1.03 \pm 0.46 \pm 0.08 \pm 0.04$	1.034 ± 0.002	1.028 ± 0.003
$[63.0, 270.0]$	$0.74 \pm 0.59 \pm 0.09 \pm 0.03$	1.043 ± 0.007	1.064 ± 0.009

Table 25. The forward-backward ratio (R_{FB}) in intervals of p_{T}^Z, together with the FSR correction. For the R_{FB} results, the first uncertainty is statistical, the second is systematic and the third is from integrated luminosity.

ϕ^*	R_{FB}	f_{FSR} (forward)	f_{FSR} (backward)
$[0.00, 0.02]$	$0.71 \pm 0.16 \pm 0.05 \pm 0.03$	1.031 ± 0.003	1.053 ± 0.003
$[0.02, 0.05]$	$0.82 \pm 0.19 \pm 0.05 \pm 0.03$	1.044 ± 0.002	1.007 ± 0.002
$[0.05, 0.10]$	$0.86 \pm 0.22 \pm 0.06 \pm 0.03$	1.010 ± 0.002	1.015 ± 0.002
$[0.10, 0.20]$	$0.75 \pm 0.19 \pm 0.05 \pm 0.03$	1.018 ± 0.001	1.014 ± 0.001
$[0.20, 0.40]$	$0.65 \pm 0.21 \pm 0.05 \pm 0.02$	1.004 ± 0.002	1.015 ± 0.002
$[0.40, 4.00]$	$0.94 \pm 0.46 \pm 0.08 \pm 0.03$	1.024 ± 0.004	1.023 ± 0.004

Table 26. The forward-backward ratio (R_{FB}) in intervals of ϕ^*, together with the FSR correction. For the R_{FB} results, the first uncertainty is statistical, the second is systematic and the third is from integrated luminosity.

	y_Z^*	$R_{p\mathrm{Pb}}$	f_{FSR}
Forward	$[2.0, 2.5]$	$0.87 \pm 0.10 \pm 0.03 \pm 0.02$	1.020 ± 0.002
	$[2.5, 3.0]$	$0.98 \pm 0.10 \pm 0.04 \pm 0.03$	1.023 ± 0.001
	$[3.0, 3.5]$	$0.89 \pm 0.13 \pm 0.03 \pm 0.02$	1.030 ± 0.001
	$[3.5, 4.0]$	$0.83 \pm 0.29 \pm 0.03 \pm 0.02$	1.014 ± 0.002
Backward	$[-4.0, -3.5]$	$0.92 \pm 0.17 \pm 0.03 \pm 0.03$	1.028 ± 0.002
	$[-3.5, -3.0]$	$1.31 \pm 0.14 \pm 0.05 \pm 0.05$	1.018 ± 0.001
	$[-3.0, -2.5]$	$1.29 \pm 0.19 \pm 0.05 \pm 0.05$	1.020 ± 0.001

Table 27. The nuclear modification factors ($R_{p\mathrm{Pb}}$) in intervals of y_Z^* for forward and backward collisions, together with the FSR correction. For the $R_{p\mathrm{Pb}}$ results, the first uncertainty is statistical, the second is systematic and the third is from integrated luminosity.

	p_{T}^{Z} [GeV]	$R_{p\mathrm{Pb}}$	f_{FSR}
Forward	$[0.0, 4.6]$	$1.04 \pm 0.15 \pm 0.04 \pm 0.03$	1.068 ± 0.002
	$[4.6, 10.5]$	$0.77 \pm 0.11 \pm 0.03 \pm 0.02$	1.033 ± 0.001
	$[10.5, 19.0]$	$0.83 \pm 0.13 \pm 0.03 \pm 0.02$	0.994 ± 0.002
	$[19.0, 34.0]$	$0.89 \pm 0.15 \pm 0.03 \pm 0.02$	0.988 ± 0.002
	$[34.0, 63.0]$	$1.34 \pm 0.25 \pm 0.06 \pm 0.04$	1.034 ± 0.002
	$[63.0, 270.0]$	$1.41 \pm 0.44 \pm 0.10 \pm 0.04$	1.043 ± 0.007
Backward	$[0.0, 4.6]$	$1.63 \pm 0.24 \pm 0.07 \pm 0.04$	1.082 ± 0.002
	$[4.6, 10.5]$	$0.76 \pm 0.17 \pm 0.03 \pm 0.02$	1.025 ± 0.002
	$[10.5, 19.0]$	$0.79 \pm 0.18 \pm 0.03 \pm 0.02$	0.976 ± 0.002
	$[19.0, 34.0]$	$1.94 \pm 0.39 \pm 0.09 \pm 0.05$	0.981 ± 0.002
	$[34.0, 63.0]$	$1.13 \pm 0.40 \pm 0.06 \pm 0.03$	1.028 ± 0.003
	$[63.0, 270.0]$	$1.63 \pm 0.98 \pm 0.11 \pm 0.04$	1.064 ± 0.009

Table 28. The nuclear modification factors ($R_{p\mathrm{Pb}}$) in intervals of p_{T}^{Z} for forward and backward collisions, together with the FSR correction. For the $R_{p\mathrm{Pb}}$ results, the first uncertainty is statistical, the second is systematic and the third is from integrated luminosity.

	ϕ^*	$R_{p\mathrm{Pb}}$	f_{FSR}
Forward	$[0.00, 0.02]$	$0.94 \pm 0.13 \pm 0.04 \pm 0.02$	1.031 ± 0.003
	$[0.02, 0.05]$	$0.82 \pm 0.11 \pm 0.03 \pm 0.02$	1.044 ± 0.002
	$[0.05, 0.10]$	$0.83 \pm 0.11 \pm 0.03 \pm 0.02$	1.010 ± 0.002
	$[0.10, 0.20]$	$0.87 \pm 0.13 \pm 0.04 \pm 0.02$	1.018 ± 0.001
	$[0.20, 0.40]$	$1.07 \pm 0.18 \pm 0.05 \pm 0.03$	1.004 ± 0.002
	$[0.40, 4.00]$	$1.52 \pm 0.29 \pm 0.09 \pm 0.04$	1.024 ± 0.004
Backward	$[0.00, 0.02]$	$1.32 \pm 0.20 \pm 0.05 \pm 0.03$	1.053 ± 0.003
	$[0.02, 0.05]$	$1.07 \pm 0.17 \pm 0.04 \pm 0.03$	1.007 ± 0.002
	$[0.05, 0.10]$	$0.94 \pm 0.17 \pm 0.04 \pm 0.02$	1.015 ± 0.002
	$[0.10, 0.20]$	$1.22 \pm 0.22 \pm 0.05 \pm 0.03$	1.014 ± 0.001
	$[0.20, 0.40]$	$1.57 \pm 0.34 \pm 0.07 \pm 0.04$	1.015 ± 0.002
	$[0.40, 4.00]$	$1.34 \pm 0.51 \pm 0.08 \pm 0.03$	1.023 ± 0.004

Table 29. The nuclear modification factors ($R_{p\mathrm{Pb}}$) in intervals of ϕ^* for forward and backward collisions, together with the FSR correction. For the $R_{p\mathrm{Pb}}$ results, the first uncertainty is statistical, the second is systematic and the third is from integrated luminosity.

References

[1] S.D. Drell and T.-M. Yan, *Massive Lepton Pair Production in Hadron-Hadron Collisions at High-Energies*, *Phys. Rev. Lett.* **25** (1970) 316 [*Erratum ibid.* **25** (1970) 902] [INSPIRE].

[2] J.C. Collins, D.E. Soper and G.F. Sterman, *Factorization of hard processes in QCD*, *Adv. Ser. Direct. High Energy Phys.* **5** (1989) 1 [`hep-ph/0409313`] [INSPIRE].

[3] G.A. Ladinsky and C.P. Yuan, *The Nonperturbative regime in QCD resummation for gauge boson production at hadron colliders*, *Phys. Rev. D* **50** (1994) R4239 [`hep-ph/9311341`] [INSPIRE].

[4] C. Balazs, J.-W. Qiu and C.P. Yuan, *Effects of QCD resummation on distributions of leptons from the decay of electroweak vector bosons*, *Phys. Lett. B* **355** (1995) 548 [`hep-ph/9505203`] [INSPIRE].

[5] C. Balazs and C.P. Yuan, *Testing multiple gluon dynamics at the Tevatron*, *Phys. Rev. Lett.* **79** (1997) 2398 [`hep-ph/9703405`] [INSPIRE].

[6] C. Balazs and C.P. Yuan, *Soft gluon effects on lepton pairs at hadron colliders*, *Phys. Rev. D* **56** (1997) 5558 [`hep-ph/9704258`] [INSPIRE].

[7] F. Landry, R. Brock, P.M. Nadolsky and C.P. Yuan, *Tevatron Run-1 Z boson data and Collins-Soper-Sterman resummation formalism*, *Phys. Rev. D* **67** (2003) 073016 [`hep-ph/0212159`] [INSPIRE].

[8] A.V. Konychev and P.M. Nadolsky, *Universality of the Collins-Soper-Sterman nonperturbative function in gauge boson production*, *Phys. Lett. B* **633** (2006) 710 [`hep-ph/0506225`] [INSPIRE].

[9] S. Camarda et al., *DYTurbo: Fast predictions for Drell-Yan processes*, *Eur. Phys. J. C* **80** (2020) 251 [*Erratum ibid.* **80** (2020) 440] [`arXiv:1910.07049`] [INSPIRE].

[10] S. Camarda, L. Cieri and G. Ferrera, *Drell–Yan lepton-pair production: qT resummation at N3LL accuracy and fiducial cross sections at N3LO*, *Phys. Rev. D* **104** (2021) L111503 [`arXiv:2103.04974`] [INSPIRE].

[11] R. Hamberg, W.L. van Neerven and T. Matsuura, *A complete calculation of the order α_s^2 correction to the Drell-Yan K factor*, *Nucl. Phys. B* **359** (1991) 343 [INSPIRE].

[12] S. Catani et al., *Vector boson production at hadron colliders: a fully exclusive QCD calculation at NNLO*, *Phys. Rev. Lett.* **103** (2009) 082001 [`arXiv:0903.2120`] [INSPIRE].

[13] K. Melnikov and F. Petriello, *Electroweak gauge boson production at hadron colliders through $O(\alpha_s^2)$*, *Phys. Rev. D* **74** (2006) 114017 [`hep-ph/0609070`] [INSPIRE].

[14] J. Rojo et al., *The PDF4LHC report on PDFs and LHC data: Results from Run I and preparation for Run II*, *J. Phys. G* **42** (2015) 103103 [`arXiv:1507.00556`] [INSPIRE].

[15] J. Butterworth et al., *PDF4LHC recommendations for LHC Run II*, *J. Phys. G* **43** (2016) 023001 [`arXiv:1510.03865`] [INSPIRE].

[16] A. Kusina et al., *Vector boson production in pPb and PbPb collisions at the LHC and its impact on nCTEQ15 PDFs*, *Eur. Phys. J. C* **77** (2017) 488 [arXiv:1610.02925] [ɪɴSPIRE].

[17] K.J. Eskola, P. Paakkinen, H. Paukkunen and C.A. Salgado, *EPPS16: Nuclear parton distributions with LHC data*, *Eur. Phys. J. C* **77** (2017) 163 [arXiv:1612.05741] [ɪɴSPIRE].

[18] D. de Florian and R. Sassot, *Nuclear parton distributions at next-to-leading order*, *Phys. Rev. D* **69** (2004) 074028 [hep-ph/0311227] [ɪɴSPIRE].

[19] M. Hirai, S. Kumano and T.-H. Nagai, *Determination of nuclear parton distribution functions and their uncertainties in next-to-leading order*, *Phys. Rev. C* **76** (2007) 065207 [arXiv:0709.3038] [ɪɴSPIRE].

[20] S. Atashbar Tehrani, *Nuclear parton densities and their uncertainties at the next-to-leading order*, *Phys. Rev. C* **86** (2012) 064301 [ɪɴSPIRE].

[21] H. Khanpour and S. Atashbar Tehrani, *Global analysis of nuclear parton distribution functions and their uncertainties at next-to-next-to-leading order*, *Phys. Rev. D* **93** (2016) 014026 [arXiv:1601.00939] [ɪɴSPIRE].

[22] S.J. Brodsky, D.S. Hwang and I. Schmidt, *Final state interactions and single spin asymmetries in semiinclusive deep inelastic scattering*, *Phys. Lett. B* **530** (2002) 99 [hep-ph/0201296] [ɪɴSPIRE].

[23] J.C. Collins, *Leading twist single transverse-spin asymmetries: Drell-Yan and deep inelastic scattering*, *Phys. Lett. B* **536** (2002) 43 [hep-ph/0204004] [ɪɴSPIRE].

[24] D. Boer, P.J. Mulders and F. Pijlman, *Universality of T odd effects in single spin and azimuthal asymmetries*, *Nucl. Phys. B* **667** (2003) 201 [hep-ph/0303034] [ɪɴSPIRE].

[25] A.V. Belitsky, X. Ji and F. Yuan, *Final state interactions and gauge invariant parton distributions*, *Nucl. Phys. B* **656** (2003) 165 [hep-ph/0208038] [ɪɴSPIRE].

[26] J.-C. Peng and J.-W. Qiu, *Novel phenomenology of parton distributions from the Drell-Yan process*, *Prog. Part. Nucl. Phys.* **76** (2014) 43 [arXiv:1401.0934] [ɪɴSPIRE].

[27] LHCʙ collaboration, *Observation of Z production in proton-lead collisions at LHCb*, *JHEP* **09** (2014) 030 [arXiv:1406.2885] [ɪɴSPIRE].

[28] CMS collaboration, *Study of Z boson production in pPb collisions at $\sqrt{s_{NN}} = 5.02$ TeV*, *Phys. Lett. B* **759** (2016) 36 [arXiv:1512.06461] [ɪɴSPIRE].

[29] ATLAS collaboration, *Z boson production in p+Pb collisions at $\sqrt{s_{NN}} = 5.02$ TeV measured with the ATLAS detector*, *Phys. Rev. C* **92** (2015) 044915 [arXiv:1507.06232] [ɪɴSPIRE].

[30] ALICE collaboration, *W and Z boson production in p-Pb collisions at $\sqrt{s_{NN}} = 5.02$ TeV*, *JHEP* **02** (2017) 077 [arXiv:1611.03002] [ɪɴSPIRE].

[31] CMS collaboration, *Study of Drell-Yan dimuon production in proton-lead collisions at $\sqrt{s_{NN}} = 8.16$ TeV*, *JHEP* **05** (2021) 182 [arXiv:2102.13648] [ɪɴSPIRE].

[32] ALICE collaboration, *Z-boson production in p-Pb collisions at $\sqrt{s_{NN}} = 8.16$ TeV and Pb-Pb collisions at $\sqrt{s_{NN}} = 5.02$ TeV*, *JHEP* **09** (2020) 076 [arXiv:2005.11126] [ɪɴSPIRE].

[33] K. Kovarik et al., *nCTEQ15 — Global analysis of nuclear parton distributions with uncertainties in the CTEQ framework*, *Phys. Rev. D* **93** (2016) 085037 [arXiv:1509.00792] [ɪɴSPIRE].

[34] M. Vesterinen and T.R. Wyatt, *A novel technique for studying the Z boson transverse momentum distribution at hadron colliders*, *Nucl. Instrum. Meth. A* **602** (2009) 432 [arXiv:0807.4956] [INSPIRE].

[35] LHCB collaboration, *The LHCb detector at the LHC*, 2008 *JINST* **3** S08005 [INSPIRE].

[36] LHCB collaboration, *LHCb detector performance*, *Int. J. Mod. Phys. A* **30** (2015) 1530022 [arXiv:1412.6352] [INSPIRE].

[37] LHCB collaboration, *Precision luminosity measurements at LHCb*, 2014 *JINST* **9** P12005 [arXiv:1410.0149] [INSPIRE].

[38] T. Sjostrand, S. Mrenna and P.Z. Skands, *A brief introduction to PYTHIA 8.1*, *Comput. Phys. Commun.* **178** (2008) 852 [arXiv:0710.3820] [INSPIRE].

[39] T. Sjostrand, S. Mrenna and P.Z. Skands, *PYTHIA 6.4 physics and manual*, *JHEP* **05** (2006) 026 [hep-ph/0603175] [INSPIRE].

[40] J. Pumplin et al., *New generation of parton distributions with uncertainties from global QCD analysis*, *JHEP* **07** (2002) 012 [hep-ph/0201195] [INSPIRE].

[41] I. Belyaev et al., *Handling of the generation of primary events in Gauss, the LHCb simulation framework*, *J. Phys. Conf. Ser.* **331** (2011) 032047 [INSPIRE].

[42] D.J. Lange, *The EvtGen particle decay simulation package*, *Nucl. Instrum. Meth. A* **462** (2001) 152 [INSPIRE].

[43] P. Golonka and Z. Was, *PHOTOS Monte Carlo: A Precision tool for QED corrections in Z and W decays*, *Eur. Phys. J. C* **45** (2006) 97 [hep-ph/0506026] [INSPIRE].

[44] T. Pierog et al., *EPOS LHC: Test of collective hadronization with data measured at the CERN Large Hadron Collider*, *Phys. Rev. C* **92** (2015) 034906 [arXiv:1306.0121] [INSPIRE].

[45] J. Allison et al., *Geant4 developments and applications*, *IEEE Trans. Nucl. Sci.* **53** (2006) 270 [INSPIRE].

[46] GEANT4 collaboration, *GEANT4 — a simulation toolkit*, *Nucl. Instrum. Meth. A* **506** (2003) 250 [INSPIRE].

[47] M. Clemencic et al., *The LHCb simulation application, Gauss: Design, evolution and experience*, *J. Phys. Conf. Ser.* **331** (2011) 032023 [INSPIRE].

[48] P. Nason, *A New method for combining NLO QCD with shower Monte Carlo algorithms*, *JHEP* **11** (2004) 040 [hep-ph/0409146] [INSPIRE].

[49] S. Frixione, P. Nason and C. Oleari, *Matching NLO QCD computations with Parton Shower simulations: the POWHEG method*, *JHEP* **11** (2007) 070 [arXiv:0709.2092] [INSPIRE].

[50] S. Alioli, P. Nason, C. Oleari and E. Re, *A general framework for implementing NLO calculations in shower Monte Carlo programs: the POWHEG BOX*, *JHEP* **06** (2010) 043 [arXiv:1002.2581] [INSPIRE].

[51] S. Alioli, P. Nason, C. Oleari and E. Re, *NLO vector-boson production matched with shower in POWHEG*, *JHEP* **07** (2008) 060 [arXiv:0805.4802] [INSPIRE].

[52] A. Buckley et al., *LHAPDF6: parton density access in the LHC precision era*, *Eur. Phys. J. C* **75** (2015) 132 [arXiv:1412.7420] [INSPIRE].

[53] S. Dulat et al., *New parton distribution functions from a global analysis of quantum chromodynamics*, *Phys. Rev. D* **93** (2016) 033006 [arXiv:1506.07443] [INSPIRE].

[54] D. Stump et al., *Inclusive jet production, parton distributions, and the search for new physics*, *JHEP* **10** (2003) 046 [hep-ph/0303013] [INSPIRE].

[55] G. Dujany and B. Storaci, *Real-time alignment and calibration of the LHCb Detector in Run II*, *J. Phys. Conf. Ser.* **664** (2015) 082010 [INSPIRE].

[56] R. Aaij et al., *The LHCb Trigger and its Performance in 2011*, 2013 *JINST* **8** P04022 [arXiv:1211.3055] [INSPIRE].

[57] R. Aaij et al., *Tesla : an application for real-time data analysis in High Energy Physics*, *Comput. Phys. Commun.* **208** (2016) 35 [arXiv:1604.05596] [INSPIRE].

[58] A. Banfi et al., *Optimisation of variables for studying dilepton transverse momentum distributions at hadron colliders*, *Eur. Phys. J. C* **71** (2011) 1600 [arXiv:1009.1580] [INSPIRE].

[59] S.J. Brodsky and H.J. Lu, *Shadowing and antishadowing of nuclear structure functions*, *Phys. Rev. Lett.* **64** (1990) 1342 [INSPIRE].

[60] EUROPEAN MUON collaboration, *The ratio of the nucleon structure functions $F2_n$ for iron and deuterium*, *Phys. Lett. B* **123** (1983) 275 [INSPIRE].

[61] LHCB collaboration, *Measurement of the forward Z boson production cross-section in pp collisions at $\sqrt{s} = 7$ TeV*, *JHEP* **08** (2015) 039 [arXiv:1505.07024] [INSPIRE].

[62] CDF collaboration, *A Measurement of $\sigma B(W \to e\nu)$ and $\sigma B(Z^0 \to e^+e-)$ in $\bar{p}p$ collisions at $\sqrt{s} = 1800$ GeV*, *Phys. Rev. D* **44** (1991) 29 [INSPIRE].

[63] ATLAS collaboration, *A search for prompt lepton-jets in pp collisions at $\sqrt{s} = 8$ TeV with the ATLAS detector*, *JHEP* **02** (2016) 062 [arXiv:1511.05542] [INSPIRE].

[64] G. Kasieczka, B. Nachman, M.D. Schwartz and D. Shih, *Automating the ABCD method with machine learning*, *Phys. Rev. D* **103** (2021) 035021 [arXiv:2007.14400] [INSPIRE].

[65] LHCB collaboration, *Measurement of the track reconstruction efficiency at LHCb*, 2015 *JINST* **10** P02007 [arXiv:1408.1251] [INSPIRE].

[66] T. Adye, *Unfolding algorithms and tests using RooUnfold*, in the proceedings of the *PHYSTAT 2011*, CERN, Geneva, (2011), p. 313–318 [DOI:10.5170/CERN-2011-006.313] [arXiv:1105.1160] [INSPIRE].

[67] G. D'Agostini, *A Multidimensional unfolding method based on Bayes' theorem*, *Nucl. Instrum. Meth. A* **362** (1995) 487 [INSPIRE].

[68] LHCB collaboration, *Measurement of forward W and Z boson production in pp collisions at $\sqrt{s} = 8$ TeV*, *JHEP* **01** (2016) 155 [arXiv:1511.08039] [INSPIRE].

[69] LHCB collaboration, *Measurement of the forward Z boson production cross-section in pp collisions at $\sqrt{s} = 13$ TeV*, *JHEP* **09** (2016) 136 [arXiv:1607.06495] [INSPIRE].

[70] LHCB collaboration, *Precision measurement of forward Z boson production in proton-proton collisions at $\sqrt{s} = 13$ TeV*, *JHEP* **07** (2022) 026 [arXiv:2112.07458] [INSPIRE].

[71] N. Davidson, T. Przedzinski and Z. Was, *PHOTOS interface in C++: technical and Physics Documentation*, *Comput. Phys. Commun.* **199** (2016) 86 [arXiv:1011.0937] [INSPIRE].

[72] A. Hocker and V. Kartvelishvili, *SVD approach to data unfolding*, *Nucl. Instrum. Meth. A* **372** (1996) 469 [hep-ph/9509307] [INSPIRE].

[73] G. Cowan, *Statistical data analysis*, Oxford University Press, Oxford, U.K. (1998).

The LHCb collaboration
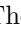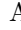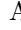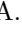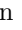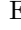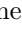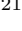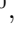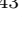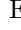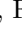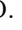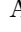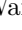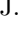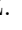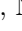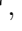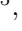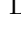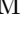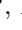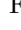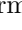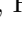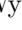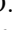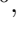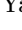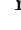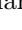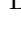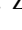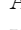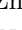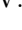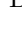
R. Aaij [32], A.S.W. Abdelmotteleb [50], C. Abellan Beteta[44], F. Abudinén [50], T. Ackernley [54], B. Adeva [40], M. Adinolfi [48], H. Afsharnia[9], C. Agapopoulou [13], C.A. Aidala [76], S. Aiola [25], Z. Ajaltouni[9], S. Akar [59], K. Akiba [32], J. Albrecht [15], F. Alessio [42], M. Alexander [53], A. Alfonso Albero [39], Z. Aliouche [56], P. Alvarez Cartelle [49], R. Amalric [13], S. Amato [2], J.L. Amey [48], Y. Amhis [11,42], L. An [42], L. Anderlini [22], M. Andersson [44], A. Andreianov [38], M. Andreotti [21], D. Andreou [62], D. Ao [6], F. Archilli [17], A. Artamonov [38], M. Artuso [62], E. Aslanides [10], M. Atzeni [44], B. Audurier [12], S. Bachmann [17], M. Bachmayer [43], J.J. Back [50], A. Bailly-reyre[13], P. Baladron Rodriguez [40], V. Balagura [12], W. Baldini [21], J. Baptista de Souza Leite [1], M. Barbetti [22,j], R.J. Barlow [56], S. Barsuk [11], W. Barter [55], M. Bartolini [49], F. Baryshnikov [38], J.M. Basels [14], G. Bassi [29,q], B. Batsukh [4], A. Battig [15], A. Bay [43], A. Beck [50], M. Becker [15], F. Bedeschi [29], I.B. Bediaga [1], A. Beiter[62], V. Belavin[38], S. Belin [40], V. Bellee [44], K. Belous [38], I. Belov [38], I. Belyaev [38], G. Bencivenni [23], E. Ben-Haim [13], A. Berezhnoy [38], R. Bernet [44], D. Berninghoff[17], H.C. Bernstein[62], C. Bertella [56], A. Bertolin [28], C. Betancourt [44], F. Betti [42], Ia. Bezshyiko [44], S. Bhasin [48], J. Bhom [35], L. Bian [67], M.S. Bieker [15], N.V. Biesuz [21], S. Bifani [47], P. Billoir [13], A. Biolchini [32], M. Birch [55], F.C.R. Bishop [49], A. Bitadze [56], A. Bizzeti [], M.P. Blago [49], T. Blake [50], F. Blanc [43], S. Blusk [62], D. Bobulska [53], J.A. Boelhauve [15], O. Boente Garcia [12], T. Boettcher [59], A. Boldyrev [38], C.S. Bolognani [73], N. Bondar [38,42], S. Borghi [56], M. Borsato [17], J.T. Borsuk [35], S.A. Bouchiba [43], T.J.V. Bowcock [54,42], A. Boyer [42], C. Bozzi [21], M.J. Bradley[55], S. Braun [60], A. Brea Rodriguez [40], J. Brodzicka [35], A. Brossa Gonzalo [50], D. Brundu [27], A. Buonaura [44], L. Buonincontri [28], A.T. Burke [56], C. Burr [42], A. Bursche[66], A. Butkevich [38], J.S. Butter [32], J. Buytaert [42], W. Byczynski [42], S. Cadeddu [27], H. Cai[67], R. Calabrese [21,i], L. Calefice [15,13], S. Cali [23], R. Calladine[47], M. Calvi [26,m], M. Calvo Gomez [74], P. Camargo Magalhaes [48], P. Campana [23], D.H. Campora Perez [73], A.F. Campoverde Quezada [6], S. Capelli [26,m], L. Capriotti [20,g], A. Carbone [20,g], G. Carboni [31], R. Cardinale [24,k], A. Cardini [27], I. Carli [4], P. Carniti [26,m], L. Carus[14], A. Casais Vidal [40], R. Caspary [17], G. Casse [54], M. Cattaneo [42], G. Cavallero [42], V. Cavallini [21,i], S. Celani [43], J. Cerasoli [10], D. Cervenkov [57], A.J. Chadwick [54], M.G. Chapman[48], M. Charles [13], Ph. Charpentier [42], C.A. Chavez Barajas [54], M. Chefdeville [8], C. Chen [3], S. Chen [4], A. Chernov [35], S. Chernyshenko [46], V. Chobanova [40], S. Cholak [43], M. Chrzaszcz [35], A. Chubykin [38], V. Chulikov [38], P. Ciambrone [23], M.F. Cicala [50], X. Cid Vidal [40], G. Ciezarek [42], G. Ciullo [i,21], P.E.L. Clarke [52], M. Clemencic [42], H.V. Cliff [49], J. Closier [42], J.L. Cobbledick [56], V. Coco [42], J.A.B. Coelho [11], J. Cogan [10], E. Cogneras [9], L. Cojocariu [37], P. Collins [42], T. Colombo [42], L. Congedo [19], A. Contu [27], N. Cooke [47], G. Coombs [53], I. Corredoira [40], G. Corti [42], B. Couturier [42], D.C. Craik [58], J. Crkovská [61], M. Cruz Torres [1,e], C.L. Da Silva [61], S. Dadabaev [38], L. Dai [65], E. Dall'Occo [15], J. Dalseno [40], C. D'Ambrosio [42], A. Danilina [38], P. d'Argent [15], J.E. Davies [56], A. Davis [56], O. De Aguiar Francisco [56], J. de Boer [42], K. De Bruyn [72], S. De Capua [56], M. De Cian [43], U. De Freitas Carneiro Da Graca [1],

E. De Lucia [23], J.M. De Miranda [1], L. De Paula [2], M. De Serio [19,f], D. De Simone [44],
P. De Simone [23], F. De Vellis [15], J.A. de Vries [73], C.T. Dean [61], F. Debernardis [19,f],
D. Decamp [8], V. Dedu [10], L. Del Buono [13], B. Delaney [58], H.-P. Dembinski [15],
V. Denysenko [44], O. Deschamps [9], F. Dettori [27,h], B. Dey [70], A. Di Cicco [23],
P. Di Nezza [23], I. Diachkov [38], S. Didenko [38], L. Dieste Maronas [40], S. Ding [62],
V. Dobishuk [46], A. Dolmatov[38], C. Dong [3], A.M. Donohoe [18], F. Dordei [27],
A.C. dos Reis [1], L. Douglas[53], A.G. Downes [8], M.W. Dudek [35], L. Dufour [42], V. Duk [71],
P. Durante [42], J.M. Durham [61], D. Dutta [56], A. Dziurda [35], A. Dzyuba [38], S. Easo [51],
U. Egede [63], V. Egorychev [38], S. Eidelman[38,†], S. Eisenhardt [52], S. Ek-In [43], L. Eklund [75],
S. Ely [62], A. Ene [37], E. Epple [61], S. Escher [14], J. Eschle [44], S. Esen [44], T. Evans [56],
L.N. Falcao [1], Y. Fan [6], B. Fang [67], S. Farry [54], D. Fazzini [26,m], M. Feo [42],
A.D. Fernez [60], F. Ferrari [20], L. Ferreira Lopes [43], F. Ferreira Rodrigues [2],
S. Ferreres Sole [32], M. Ferrillo [44], M. Ferro-Luzzi [42], S. Filippov [38], R.A. Fini [19],
M. Fiorini [21,i], M. Firlej [34], K.M. Fischer [57], D.S. Fitzgerald [76], C. Fitzpatrick [56],
T. Fiutowski [34], F. Fleuret [12], M. Fontana [13], F. Fontanelli [24,k], R. Forty [42],
D. Foulds-Holt [49], V. Franco Lima [54], M. Franco Sevilla [60], M. Frank [42], E. Franzoso [21,i],
G. Frau [17], C. Frei [42], D.A. Friday [53], J. Fu [6], Q. Fuehring [15], E. Gabriel [32],
G. Galati [19,f], M.D. Galati [72], A. Gallas Torreira [40], D. Galli [20,g], S. Gambetta [52,42],
Y. Gan [3], M. Gandelman [2], P. Gandini [25], Y. Gao [5], M. Garau [27,h],
L.M. Garcia Martin [50], P. Garcia Moreno [39], J. García Pardiñas [26,m], B. Garcia Plana[40],
F.A. Garcia Rosales [12], L. Garrido [39], C. Gaspar [42], R.E. Geertsema [32], D. Gerick[17],
L.L. Gerken [15], E. Gersabeck [56], M. Gersabeck [56], T. Gershon [50], L. Giambastiani [28],
V. Gibson [49], H.K. Giemza [36], A.L. Gilman [57], M. Giovannetti [23,t], A. Gioventù [40],
P. Gironella Gironell [39], C. Giugliano [21,i], M.A. Giza [35], K. Gizdov [52],
E.L. Gkougkousis [42], V.V. Gligorov [13,42], C. Göbel [64], E. Golobardes [74], D. Golubkov [38],
A. Golutvin [55,38], A. Gomes [1,a], S. Gomez Fernandez [39], F. Goncalves Abrantes [57],
M. Goncerz [35], G. Gong [3], I.V. Gorelov [38], C. Gotti [26], J.P. Grabowski [17],
T. Grammatico [13], L.A. Granado Cardoso [42], E. Graugés [39], E. Graverini [43], G. Graziani [],
A. T. Grecu [37], L.M. Greeven [32], N.A. Grieser [4], L. Grillo [53], S. Gromov [38],
B.R. Gruberg Cazon [57], C. Gu [3], M. Guarise [21,i], M. Guittiere [11], P. A. Günther [17],
E. Gushchin [38], A. Guth[14], Y. Guz [38], T. Gys [42], T. Hadavizadeh [63], G. Haefeli [43],
C. Haen [42], J. Haimberger [42], S.C. Haines [49], T. Halewood-leagas [54], M.M. Halvorsen [42],
P.M. Hamilton [60], J. Hammerich [54], Q. Han [7], X. Han [17], E.B. Hansen [56],
S. Hansmann-Menzemer [17,42], L. Hao [6], N. Harnew [57], T. Harrison [54], C. Hasse [42],
M. Hatch [42], J. He [6,c], K. Heijhoff [32], K. Heinicke [15], R.D.L. Henderson [63,50],
A.M. Hennequin [58], K. Hennessy [54], L. Henry [42], J. Heuel [14], A. Hicheur [2], D. Hill [43],
M. Hilton [56], S.E. Hollitt [15], R. Hou [7], Y. Hou [8], J. Hu[17], J. Hu [66], W. Hu [5], X. Hu [3],
W. Huang [6], X. Huang[67], W. Hulsbergen [32], R.J. Hunter [50], M. Hushchyn [38],
D. Hutchcroft [54], P. Ibis [15], M. Idzik [34], D. Ilin [38], P. Ilten [59], A. Inglessi [38],
A. Iniukhin [38], A. Ishteev [38], K. Ivshin [38], R. Jacobsson [42], H. Jage [14],
S.J. Jaimes Elles [41], S. Jakobsen [42], E. Jans [32], B.K. Jashal [41], A. Jawahery [60],
V. Jevtic [15], X. Jiang [4,6], Y. Jiang [6], M. John [57], D. Johnson [58], C.R. Jones [49],
T.P. Jones [50], B. Jost [42], N. Jurik [42], I. Juszczak [35], S. Kandybei [45], Y. Kang [3],

M. Karacson [42], D. Karpenkov [38], M. Karpov [38], J.W. Kautz [59], F. Keizer [42],
D.M. Keller [62], M. Kenzie [50], T. Ketel [33], B. Khanji [15], A. Kharisova [38],
S. Kholodenko [38], T. Kirn [14], V.S. Kirsebom [43], O. Kitouni [58], S. Klaver [33],
N. Kleijne [29,q], K. Klimaszewski [36], M.R. Kmiec [36], S. Koliiev [46], A. Kondybayeva [38],
A. Konoplyannikov [38], P. Kopciewicz [34], R. Kopecna [17], P. Koppenburg [32], M. Korolev [38],
I. Kostiuk [32,46], O. Kot [46], S. Kotriakhova [], A. Kozachuk [38], P. Kravchenko [38],
L. Kravchuk [38], R.D. Krawczyk [42], M. Kreps [50], S. Kretzschmar [14], P. Krokovny [38],
W. Krupa [34], W. Krzemien [36], J. Kubat [17], W. Kucewicz [35,34], M. Kucharczyk [35],
V. Kudryavtsev [38], G.J. Kunde [61], D. Lacarrere [42], G. Lafferty [56], A. Lai [27],
A. Lampis [27,h], D. Lancierini [44], J.J. Lane [56], R. Lane [48], G. Lanfranchi [23],
C. Langenbruch [14], J. Langer [15], O. Lantwin [38], T. Latham [50], F. Lazzari [29,u],
M. Lazzaroni [25,l], R. Le Gac [10], S.H. Lee [76], R. Lefèvre [9], A. Leflat [38], S. Legotin [38],
P. Lenisa [i,21], O. Leroy [10], T. Lesiak [35], B. Leverington [17], H. Li [66], K. Li [7], P. Li [17],
S. Li [7], T. Li [66], Y. Li [4], Z. Li [62], X. Liang [62], C. Lin [6], T. Lin [51], R. Lindner [42],
V. Lisovskyi [15], R. Litvinov [27,h], G. Liu [66], H. Liu [6], Q. Liu [6], S. Liu [4,6],
A. Lobo Salvia [39], A. Loi [27], R. Lollini [71], J. Lomba Castro [40], I. Longstaff [53],
J.H. Lopes [2], S. López Soliño [40], G.H. Lovell [49], Y. Lu [4,b], C. Lucarelli [22,j],
D. Lucchesi [28,o], S. Luchuk [38], M. Lucio Martinez [32], V. Lukashenko [32,46], Y. Luo [3],
A. Lupato [56], E. Luppi [21,i], A. Lusiani [29,q], K. Lynch [18], X.-R. Lyu [6], L. Ma [4], R. Ma [66],
R. Ma [6], S. Maccolini [20], F. Machefert [11], F. Maciuc [37], V. Macko [43], P. Mackowiak [15],
S. Maddrell-Mander [48], L.R. Madhan Mohan [48], A. Maevskiy [38], D. Maisuzenko [38],
M.W. Majewski [34], J.J. Malczewski [35], S. Malde [57], B. Malecki [35,42], A. Malinin [38],
T. Maltsev [38], H. Malygina [17], G. Manca [27,h], G. Mancinelli [10], D. Manuzzi [20],
C.A. Manzari [44], D. Marangotto [25,l], J.F. Marchand [8], U. Marconi [20], S. Mariani [22,j],
C. Marin Benito [39], M. Marinangeli [43], J. Marks [17], A.M. Marshall [48], P.J. Marshall [54],
G. Martelli [71,p], G. Martellotti [30], L. Martinazzoli [42,m], M. Martinelli [26,m],
D. Martinez Santos [40], F. Martinez Vidal [41], A. Massafferri [1], M. Materok [14], R. Matev [42],
A. Mathad [44], V. Matiunin [38], C. Matteuzzi [26], K.R. Mattioli [76], A. Mauri [32],
E. Maurice [12], J. Mauricio [39], M. Mazurek [42], M. McCann [55], L. Mcconnell [18],
T.H. McGrath [56], N.T. McHugh [53], A. McNab [56], R. McNulty [18], J.V. Mead [54],
B. Meadows [59], G. Meier [15], D. Melnychuk [36], S. Meloni [26,m], M. Merk [32,73],
A. Merli [25,l], L. Meyer Garcia [2], D. Miao [4,6], M. Mikhasenko [69,d], D.A. Milanes [68],
E. Millard [50], M. Milovanovic [42], M.-N. Minard [8,†], A. Minotti [26,m], S.E. Mitchell [52],
B. Mitreska [56], D.S. Mitzel [15], A. Mödden [15], R.A. Mohammed [57], R.D. Moise [55],
S. Mokhnenko [38], T. Mombächer [40], I.A. Monroy [68], S. Monteil [9], M. Morandin [28],
G. Morello [23], M.J. Morello [29,q], J. Moron [34], A.B. Morris [69], A.G. Morris [50],
R. Mountain [62], H. Mu [3], F. Muheim [52], M. Mulder [72], K. Müller [44], C.H. Murphy [57],
D. Murray [56], R. Murta [55], P. Muzzetto [27,h], P. Naik [48], T. Nakada [43],
R. Nandakumar [51], T. Nanut [42], I. Nasteva [2], M. Needham [52], N. Neri [25,l],
S. Neubert [69], N. Neufeld [42], P. Neustroev [38], R. Newcombe [55], E.M. Niel [43], S. Nieswand [14],
N. Nikitin [38], N.S. Nolte [58], C. Normand [8,h,27], C. Nunez [76], A. Oblakowska-Mucha [34],
V. Obraztsov [38], T. Oeser [14], D.P. O'Hanlon [48], S. Okamura [21,i], R. Oldeman [27,h],
F. Oliva [52], M.E. Olivares [62], C.J.G. Onderwater [72], R.H. O'Neil [52],

J.M. Otalora Goicochea [2], T. Ovsiannikova [38], P. Owen [44], A. Oyanguren [41],
O. Ozcelik [52], K.O. Padeken [69], B. Pagare [50], P.R. Pais [42], T. Pajero [57], A. Palano [19],
M. Palutan [23], Y. Pan [56], G. Panshin [38], A. Papanestis [51], M. Pappagallo [19,f],
L.L. Pappalardo [21,i], C. Pappenheimer [59], W. Parker [60], C. Parkes [56], B. Passalacqua [21,i],
G. Passaleva [22], A. Pastore [19], M. Patel [55], C. Patrignani [20,g], C.J. Pawley [73],
A. Pearce [42], A. Pellegrino [32], M. Pepe Altarelli [42], S. Perazzini [20], D. Pereima [38],
A. Pereiro Castro [40], P. Perret [9], M. Petric [53], K. Petridis [48], A. Petrolini [24,k], A. Petrov[38],
S. Petrucci [52], M. Petruzzo [25], H. Pham [62], A. Philippov [38], R. Piandani [6], L. Pica [29,q],
M. Piccini [71], B. Pietrzyk [8], G. Pietrzyk [11], M. Pili [57], D. Pinci [30], F. Pisani [42],
M. Pizzichemi [26,m,42], V. Placinta [37], J. Plews [47], M. Plo Casasus [40], F. Polci [13,42],
M. Poli Lener [23], M. Poliakova[62], A. Poluektov [10], N. Polukhina [38], I. Polyakov [42],
E. Polycarpo [2], S. Ponce [42], D. Popov [6,42], S. Popov [38], S. Poslavskii [38], K. Prasanth [35],
L. Promberger [42], C. Prouve [40], V. Pugatch [46], V. Puill [11], G. Punzi [29,r], H.R. Qi [3],
W. Qian [6], N. Qin [3], S. Qu [3], R. Quagliani [43], N.V. Raab [18], R.I. Rabadan Trejo [6],
B. Rachwal [34], J.H. Rademacker [48], R. Rajagopalan[62], M. Rama [29], M. Ramos Pernas [50],
M.S. Rangel [2], F. Ratnikov [38], G. Raven [33,42], M. Rebollo De Miguel [41], F. Redi [42],
F. Reiss [56], C. Remon Alepuz[41], Z. Ren [3], V. Renaudin [57], P.K. Resmi [10], R. Ribatti [29,q],
A.M. Ricci [27], S. Ricciardi [51], K. Rinnert [54], P. Robbe [11], G. Robertson [52],
A.B. Rodrigues [43], E. Rodrigues [54], J.A. Rodriguez Lopez [68], E. Rodriguez Rodriguez [40],
A. Rollings [57], P. Roloff [42], V. Romanovskiy [38], M. Romero Lamas [40], A. Romero Vidal [40],
J.D. Roth[76,†], M. Rotondo [23], M.S. Rudolph [62], T. Ruf [42], R.A. Ruiz Fernandez [40],
J. Ruiz Vidal[41], A. Ryzhikov [38], J. Ryzka [34], J.J. Saborido Silva [40], N. Sagidova [38],
N. Sahoo [47], B. Saitta [27,h], M. Salomoni [42], C. Sanchez Gras [32], I. Sanderswood [41],
R. Santacesaria [30], C. Santamarina Rios [40], M. Santimaria [23], E. Santovetti [31,t],
D. Saranin [38], G. Sarpis [14], M. Sarpis [69], A. Sarti [30], C. Satriano [30,s], A. Satta [31],
M. Saur [15], D. Savrina [38], H. Sazak [9], L.G. Scantlebury Smead [57], A. Scarabotto [13],
S. Schael [14], S. Scherl [54], M. Schiller [53], H. Schindler [42], M. Schmelling [16], B. Schmidt [42],
S. Schmitt [14], O. Schneider [43], A. Schopper [42], M. Schubiger [32], S. Schulte [43],
M.H. Schune [11], R. Schwemmer [42], B. Sciascia [23,42], A. Sciuccati [42], S. Sellam [40],
A. Semennikov [38], M. Senghi Soares [33], A. Sergi [24,k], N. Serra [44], L. Sestini [28],
A. Seuthe [15], Y. Shang [5], D.M. Shangase [76], M. Shapkin [38], I. Shchemerov [38],
L. Shchutska [43], T. Shears [54], L. Shekhtman [38], Z. Shen [5], S. Sheng [4,6],
V. Shevchenko [38], B. Shi [6], E.B. Shields [26,m], Y. Shimizu [11], E. Shmanin [38],
J.D. Shupperd [62], B.G. Siddi [21,i], R. Silva Coutinho [44], G. Simi [28], S. Simone [19,f],
M. Singla [63], N. Skidmore [56], R. Skuza [17], T. Skwarnicki [62], M.W. Slater [47],
I. Slazyk [21,i], J.C. Smallwood [57], J.G. Smeaton [49], E. Smith [44], M. Smith [55],
A. Snoch [32], L. Soares Lavra [9], M.D. Sokoloff [59], F.J.P. Soler [53], A. Solomin [38,48],
A. Solovev [38], I. Solovyev [38], F.L. Souza De Almeida [2], B. Souza De Paula [2], B. Spaan[15,†],
E. Spadaro Norella [25,l], E. Spiridenkov[38], P. Spradlin [53], V. Sriskaran [42], F. Stagni [42],
M. Stahl [59], S. Stahl [42], S. Stanislaus [57], E.N. Stein [42], O. Steinkamp [44], O. Stenyakin[38],
H. Stevens [15], S. Stone [62,†], D. Strekalina [38], F. Suljik [57], J. Sun [27], L. Sun [67],
Y. Sun [60], P. Svihra [56], P.N. Swallow [47], K. Swientek [34], A. Szabelski [36], T. Szumlak [34],
M. Szymanski [42], Y. Tan [3], S. Taneja [56], A.R. Tanner[48], M.D. Tat [57], A. Terentev [38],

F. Teubert [42], E. Thomas [42], D.J.D. Thompson [47], K.A. Thomson [54], H. Tilquin [55],
V. Tisserand [9], S. T'Jampens [8], M. Tobin [4], L. Tomassetti [21,i], G. Tonani [25,l], X. Tong [5],
D. Torres Machado [1], D.Y. Tou [3], E. Trifonova[38], S.M. Trilov [48], C. Trippl [43], G. Tuci [6],
A. Tully [43], N. Tuning [32,42], A. Ukleja [36], D.J. Unverzagt [17], E. Ursov[38], A. Usachov [32],
A. Ustyuzhanin [38], U. Uwer [17], A. Vagner[38], V. Vagnoni [20], A. Valassi [42], G. Valenti [20],
N. Valls Canudas [74], M. van Beuzekom [32], M. Van Dijk [43], H. Van Hecke [61],
E. van Herwijnen [38], M. van Veghel [72], R. Vazquez Gomez [39], P. Vazquez Regueiro [40],
C. Vázquez Sierra [42], S. Vecchi [21], J.J. Velthuis [48], M. Veltri [22,v], A. Venkateswaran [62],
M. Veronesi [32], M. Vesterinen [50], D. Vieira [59], M. Vieites Diaz [43], X. Vilasis-Cardona [74],
E. Vilella Figueras [54], A. Villa [20], P. Vincent [13], F.C. Volle [11], D. vom Bruch [10],
A. Vorobyev[38], V. Vorobyev[38], N. Voropaev [38], K. Vos [73], R. Waldi [17], J. Walsh [29],
G. Wan [5], C. Wang [17], J. Wang [5], J. Wang [4], J. Wang [3], J. Wang [67], M. Wang [5],
R. Wang [48], X. Wang [66], Y. Wang [7], Z. Wang [44], Z. Wang [3], Z. Wang [6],
J.A. Ward [50,63], N.K. Watson [47], D. Websdale [55], C. Weisser[58], B.D.C. Westhenry [48],
D.J. White [56], M. Whitehead [53], A.R. Wiederhold [50], D. Wiedner [15], G. Wilkinson [57],
M.K. Wilkinson [59], I. Williams[49], M. Williams [58], M.R.J. Williams [52], R. Williams [49],
F.F. Wilson [51], W. Wislicki [36], M. Witek [35], L. Witola [17], C.P. Wong [61], G. Wormser [11],
S.A. Wotton [49], H. Wu [62], K. Wyllie [42], S. Xian[66], Z. Xiang [6], D. Xiao [7], Y. Xie [7],
A. Xu [5], J. Xu [6], L. Xu [3], M. Xu [50], Q. Xu[6], Z. Xu [9], Z. Xu [6], D. Yang [3], S. Yang [6],
Y. Yang [6], Z. Yang [5], Z. Yang [60], L.E. Yeomans [54], H. Yin [7], J. Yu [65], X. Yuan [62],
E. Zaffaroni [43], M. Zavertyaev [16], M. Zdybal [35], O. Zenaiev [42], M. Zeng [3], D. Zhang [7],
L. Zhang [3], S. Zhang [65], S. Zhang [5], Y. Zhang [5], Y. Zhang[57], A. Zharkova [38],
A. Zhelezov [17], Y. Zheng [6], T. Zhou [5], X. Zhou [6], Y. Zhou [6], V. Zhovkovska [11], Q. Zhu[3],
X. Zhu [3], X. Zhu [7], Z. Zhu [6], V. Zhukov [14,38], Q. Zou [4,6], S. Zucchelli [20,g],
D. Zuliani [28], G. Zunica [56]

1 Centro Brasileiro de Pesquisas Físicas (CBPF), Rio de Janeiro, Brazil
2 Universidade Federal do Rio de Janeiro (UFRJ), Rio de Janeiro, Brazil
3 Center for High Energy Physics, Tsinghua University, Beijing, China
4 Institute Of High Energy Physics (IHEP), Beijing, China
5 School of Physics State Key Laboratory of Nuclear Physics and Technology, Peking University, Beijing, China
6 University of Chinese Academy of Sciences, Beijing, China
7 Institute of Particle Physics, Central China Normal University, Wuhan, Hubei, China
8 Université Savoie Mont Blanc, CNRS, IN2P3-LAPP, Annecy, France
9 Université Clermont Auvergne, CNRS/IN2P3, LPC, Clermont-Ferrand, France
10 Aix Marseille Univ, CNRS/IN2P3, CPPM, Marseille, France
11 Université Paris-Saclay, CNRS/IN2P3, IJCLab, Orsay, France
12 Laboratoire Leprince-Ringuet, CNRS/IN2P3, Ecole Polytechnique, Institut Polytechnique de Paris, Palaiseau, France
13 LPNHE, Sorbonne Université, Paris Diderot Sorbonne Paris Cité, CNRS/IN2P3, Paris, France
14 I. Physikalisches Institut, RWTH Aachen University, Aachen, Germany
15 Fakultät Physik, Technische Universität Dortmund, Dortmund, Germany
16 Max-Planck-Institut für Kernphysik (MPIK), Heidelberg, Germany
17 Physikalisches Institut, Ruprecht-Karls-Universität Heidelberg, Heidelberg, Germany
18 School of Physics, University College Dublin, Dublin, Ireland
19 INFN Sezione di Bari, Bari, Italy

[20] INFN Sezione di Bologna, Bologna, Italy

[21] INFN Sezione di Ferrara, Ferrara, Italy

[22] INFN Sezione di Firenze, Firenze, Italy

[23] INFN Laboratori Nazionali di Frascati, Frascati, Italy

[24] INFN Sezione di Genova, Genova, Italy

[25] INFN Sezione di Milano, Milano, Italy

[26] INFN Sezione di Milano-Bicocca, Milano, Italy

[27] INFN Sezione di Cagliari, Monserrato, Italy

[28] Università degli Studi di Padova, Università e INFN, Padova, Padova, Italy

[29] INFN Sezione di Pisa, Pisa, Italy

[30] INFN Sezione di Roma La Sapienza, Roma, Italy

[31] INFN Sezione di Roma Tor Vergata, Roma, Italy

[32] Nikhef National Institute for Subatomic Physics, Amsterdam, Netherlands

[33] Nikhef National Institute for Subatomic Physics and VU University Amsterdam, Amsterdam, Netherlands

[34] AGH — University of Science and Technology, Faculty of Physics and Applied Computer Science, Kraków, Poland

[35] Henryk Niewodniczanski Institute of Nuclear Physics Polish Academy of Sciences, Kraków, Poland

[36] National Center for Nuclear Research (NCBJ), Warsaw, Poland

[37] Horia Hulubei National Institute of Physics and Nuclear Engineering, Bucharest-Magurele, Romania

[38] Affiliated with an institute covered by a cooperation agreement with CERN

[39] ICCUB, Universitat de Barcelona, Barcelona, Spain

[40] Instituto Galego de Física de Altas Enerxías (IGFAE), Universidade de Santiago de Compostela, Santiago de Compostela, Spain

[41] Instituto de Fisica Corpuscular, Centro Mixto Universidad de Valencia — CSIC, Valencia, Spain

[42] European Organization for Nuclear Research (CERN), Geneva, Switzerland

[43] Institute of Physics, Ecole Polytechnique Fédérale de Lausanne (EPFL), Lausanne, Switzerland

[44] Physik-Institut, Universität Zürich, Zürich, Switzerland

[45] NSC Kharkiv Institute of Physics and Technology (NSC KIPT), Kharkiv, Ukraine

[46] Institute for Nuclear Research of the National Academy of Sciences (KINR), Kyiv, Ukraine

[47] University of Birmingham, Birmingham, United Kingdom

[48] H.H. Wills Physics Laboratory, University of Bristol, Bristol, United Kingdom

[49] Cavendish Laboratory, University of Cambridge, Cambridge, United Kingdom

[50] Department of Physics, University of Warwick, Coventry, United Kingdom

[51] STFC Rutherford Appleton Laboratory, Didcot, United Kingdom

[52] School of Physics and Astronomy, University of Edinburgh, Edinburgh, United Kingdom

[53] School of Physics and Astronomy, University of Glasgow, Glasgow, United Kingdom

[54] Oliver Lodge Laboratory, University of Liverpool, Liverpool, United Kingdom

[55] Imperial College London, London, United Kingdom

[56] Department of Physics and Astronomy, University of Manchester, Manchester, United Kingdom

[57] Department of Physics, University of Oxford, Oxford, United Kingdom

[58] Massachusetts Institute of Technology, Cambridge, MA, United States

[59] University of Cincinnati, Cincinnati, OH, United States

[60] University of Maryland, College Park, MD, United States

[61] Los Alamos National Laboratory (LANL), Los Alamos, NM, United States

[62] Syracuse University, Syracuse, NY, United States

[63] School of Physics and Astronomy, Monash University, Melbourne, Australia, associated to [50]

[64] Pontifícia Universidade Católica do Rio de Janeiro (PUC-Rio), Rio de Janeiro, Brazil, associated to [2]

[65] Physics and Micro Electronic College, Hunan University, Changsha City, China, associated to [7]

[66] Guangdong Provincial Key Laboratory of Nuclear Science, Guangdong-Hong Kong Joint Laboratory of Quantum Matter, Institute of Quantum Matter, South China Normal University, Guangzhou, China, associated to [3]

[67] *School of Physics and Technology, Wuhan University, Wuhan, China, associated to [3]*

[68] *Departamento de Fisica , Universidad Nacional de Colombia, Bogota, Colombia, associated to [13]*

[69] *Universität Bonn — Helmholtz-Institut für Strahlen und Kernphysik, Bonn, Germany, associated to [17]*

[70] *Eotvos Lorand University, Budapest, Hungary, associated to [42]*

[71] *INFN Sezione di Perugia, Perugia, Italy, associated to [21]*

[72] *Van Swinderen Institute, University of Groningen, Groningen, Netherlands, associated to [32]*

[73] *Universiteit Maastricht, Maastricht, Netherlands, associated to [32]*

[74] *DS4DS, La Salle, Universitat Ramon Llull, Barcelona, Spain, associated to [39]*

[75] *Department of Physics and Astronomy, Uppsala University, Uppsala, Sweden, associated to [53]*

[76] *University of Michigan, Ann Arbor, MI, United States, associated to [62]*

[a] *Universidade Federal do Triângulo Mineiro (UFTM), Uberaba-MG, Brazil*

[b] *Central South U., Changsha, China*

[c] *Hangzhou Institute for Advanced Study, UCAS, Hangzhou, China*

[d] *Excellence Cluster ORIGINS, Munich, Germany*

[e] *Universidad Nacional Autónoma de Honduras, Tegucigalpa, Honduras*

[f] *Università di Bari, Bari, Italy*

[g] *Università di Bologna, Bologna, Italy*

[h] *Università di Cagliari, Cagliari, Italy*

[i] *Università di Ferrara, Ferrara, Italy*

[j] *Università di Firenze, Firenze, Italy*

[k] *Università di Genova, Genova, Italy*

[l] *Università degli Studi di Milano, Milano, Italy*

[m] *Università di Milano Bicocca, Milano, Italy*

[n] *Università di Modena e Reggio Emilia, Modena, Italy*

[o] *Università di Padova, Padova, Italy*

[p] *Università di Perugia, Perugia, Italy*

[q] *Scuola Normale Superiore, Pisa, Italy*

[r] *Università di Pisa, Pisa, Italy*

[s] *Università della Basilicata, Potenza, Italy*

[t] *Università di Roma Tor Vergata, Roma, Italy*

[u] *Università di Siena, Siena, Italy*

[v] *Università di Urbino, Urbino, Italy*

[†] *Deceased*